Overcalcified forms of the coccolithophore *Emiliania huxleyi* in high CO_2 waters are not pre-adapted to ocean acidification.

Peter von Dassow[1,2,3*], Francisco Díaz-Rosas[1,2], El Mahdi Bendif[4], Juan-Diego Gaitán-Espitia[5], Daniella Mella-Flores[1], Sebastian Rokitta[6], Uwe John[6], and Rodrigo Torres[7,8]

[1] Facultad de Ciencias Biológicas, Pontificia Universidad Católica de Chile, Santiago, Chile.
[2] Instituto Milenio de Oceanografía de Chile.
[3] UMI 3614, Evolutionary Biology and Ecology of Algae, CNRS-UPMC Sorbonne Universités, PUCCh, UACH.
[4] Department of Plant Sciences, University of Oxford, OX1 3RB Oxford, UK.
[5] CSIRO Oceans and Atmosphere, GPO Box 1538, Hobart 7001, TAS, Australia.
[6] Alfred Wegener Institute – Helmholtz Centre for Polar and Marine Research, Bremerhaven, Germany.
[7] Centro de Investigación en Ecosistemas de la Patagonia (CIEP), Coyhaique, Chile.
[8] Centro de Investigación: Dinámica de Ecosistemas marinos de Altas Latitudes (IDEAL), Punta Arenas, Chile.

Correspondence to: Peter von Dassow (pvondassow@bio.puc.cl)

Abstract. Marine multicellular organisms inhabiting waters with natural high fluctuations in pH appear more tolerant to acidification than conspecifics occurring in nearby stable waters, suggesting that environments of fluctuating pH hold genetic reservoirs for adaptation of key groups to ocean acidification (OA). The abundant and cosmopolitan calcifying phytoplankton *Emiliania huxleyi* exhibits a range of morphotypes with varying degrees of coccolith mineralization. We show that *E. huxleyi* populations in the naturally acidified upwelling waters of the Eastern South Pacific, where pH drops below 7.8 as is predicted for the global surface ocean by the year 2100, are dominated by exceptionally overcalcified morphotypes whose distal coccolith shield can be almost solid calcite. Shifts in morphotype composition of *E. huxleyi* populations correlate with changes in carbonate system parameters. We tested if these correlations indicate that the hypercalcified morphotype is adapted to OA. In experimental exposures to present-day vs. future pCO_2 (400 µatm vs. 1200 µatm), the overcalcified morphotypes showed the same growth inhibition (-29.1±6.3%) as moderately calcified morphotypes isolated from non-acidified water (-30.7±8.8%). Under the high CO_2/low pH condition, production rates of particulate organic carbon (POC) increased, while production rates of particulate inorganic carbon (PIC) were maintained or decreased slightly (but not significantly), leading to lowered PIC/POC ratios in all strains. There were no consistent correlations of response intensity with strain origin. The high CO_2/low pH condition affected coccolith morphology equally or more strongly in overcalcified strains compared to moderately calcified strains. High CO_2/low pH conditions appear not to directly select for exceptionally overcalcified morphotypes over other morphotypes directly, but perhaps indirectly by ecologically correlated factors. More generally, these results suggest that oceanic planktonic microorganisms, despite their rapid turn-over and large population sizes, do not necessarily exhibit adaptations to naturally high CO_2 upwellings, and this ubiquitous coccolithophore may be near a limit of its capacity to adapt to ongoing ocean acidification.

1 Introduction

Coccolithophores are planktonic single-celled photoautotrophs mostly in the range 3-20 µm and characterized by bearing calcite plates (coccoliths) (Tyrrell and Young, 2009) and represent one of the most abundant and widespread groups of marine eukaryotic phytoplankton (Iglesias-Rodríguez et al., 2002; Litchman et al., 2015). In addition to being important primary producers, coccolithophores contribute most of the calcium carbonate ($CaCO_3$) precipitation in pelagic systems. Although $CaCO_3$ precipitation in the surface is a source of CO_2, i.e., the 'carbonate counter pump' (Frankignoulle et al., 1994), $CaCO_3$ may enhance sinking of organic matter by imposing a ballast effect on sinking aggregates (Armstrong et al., 2002; Sanders et al., 2010). Thus, this plankton functional group has a complex role in ocean carbon cycles. Roughly a third of current anthropogenic CO_2 emissions are being absorbed in the ocean (Sabine et al., 2004), driving a decrease in pH, the

Deleted: Marine Biogeosciences | PhytoChange

Deleted: OA

Deleted: s

Deleted: OA

Deleted: OA

Deleted: and its dissolution at depth may consume more CO_2 than is released at the surface (Smith, 2013)

conversion of CO_3^{2-} to HCO_3^-, and a drop in saturation states of the $CaCO_3$ minerals aragonite and calcite (Ω_A, Ω_C), phenomena collectively termed ocean acidification (OA, Orr et al., 2005). Although most surface waters are expected to remain super-saturated with respect to calcite (Ω_C>1), which is less soluble than aragonite, the drop in Ω_C might still result in decreases in calcite biomineralization (Hofmann and Schellnhuber, 2009). Understanding the response of coccolithophores to OA is thus needed for predicting how pelagic ecosystems and the relative intensity of the biological carbon pumps will change as atmospheric CO_2 continues to increase.

Many studies designed to assess coccolithophores´ responses to low pH have been performed in short-term culture and mesocosm experiments on time-scales of weeks to months, and carbonate systems were usually manipulated to mimic pre-industrial, present and future CO_2 levels. Mesocosm studies have shown that North Sea populations of the cosmopolitan and abundant species *Emiliania huxleyi* are negatively impacted by low pH conditions (Engel et al., 2005; Riebesell et al., 2017). However, a wide range of growth, calcification (PIC) and productivity (POC) responses to have been reported in laboratory cultures of *E. huxleyi*, mostly using different regional strains (Riebesell et al., 2000; Iglesias-Rodriguez et al., 2008; Langer et al., 2009; Müller et al., 2015a, 2017; Brady Olson et al., 2017; Jin et al., 2017). According to a recent comprehensive review and meta-analysis (Meyer and Riebesell, 2015), the mean responses of *E. huxleyi* averaged over 19 studies indicated that high CO_2/low pH conditions have a negative effect on PIC quotas and production rates as well as PIC/POC ratios, but no consistent effects on POC quotas and production rates. The response variability among strains of *E. huxleyi* (Langer et al., 2009; Müller et al., 2015a) is also seen within the genus *Calcidiscus* (Diner et al., 2015), and suggests a high potential for genetic adaptation within coccolithophores.

Such adaptive capacity to high CO_2/low pH conditions has been suggested for *E. huxleyi* in lab-based long-term experimental evolution studies (up to 2000 generations) on clonal strains (Lohbeck et al., 2012; Schlüter et al., 2016). It is still difficult to know to which extent such experiments reflect real-world adaptation processes. First, only asexually propagating cells have yet been explored in the lab, while sexual recombination in natural populations is expected to accelerate adaptation (McDonald et al., 2016). Second, calcification is costly and in nature must be maintained by providing benefits to the cell. What these benefits are remains unclear. It has been suggested that coccoliths may provide defense against grazing or parasites, modify light/UV levels reaching the cell, amongst other proposed functions (Monteiro et al., 2016). The benefits of calcification likely vary among species, and may have changed over the course of evolution or with environmental change. For example, in paleo-oceans, it might have helped alleviate toxicity from Ca2+ when levels reached up to four-fold higher than in the modern ocean during the Cretaceous (Müller et al., 2015b). The long-term and non-linear declines in calcification observed in experimental adaptation to high high CO_2/low pH (Schlüter et al., 2016) thus might have a high potential cost if such changes occurred in nature.

Complementary to experimental approaches, observational studies that correlate coccolithophore communities and levels or rates of calcification with variability in carbonate system parameters offer important insights into possible adaptations to high CO_2/low pH. Focusing only on *E. huxleyi* and the closely related genus *Gephyrocapsa* (both within the family Noëlaerhabdaceae), a general pattern has been documented of a decreasing calcite mass of coccoliths and coccospheres with increasing pCO_2 both modern and recent fossil coccolithophores across the world´s ocean basins (Beaufort et al., 2011). This pattern involved shifts away from more heavily calcified *Gephyrocapsa* that dominated assemblages under the lowest pCO_2, towards a spectrum of *E. huxleyi* morphotypes that were more abundant under intermediate and high pCO_2: *E. huxleyi* 'type A' morphotypes with heavier coccoliths (more calcite per coccolith) dominated *E. huxleyi* populations in waters with intermediate pCO_2 while 'type B/C' or 'type C' morphotypes with successively lighter coccoliths, dominated in higher pCO_2 waters (Beaufort et al., 2011; Poulton et al., 2011).

Beyond this comparably clear pattern, the survey by Beaufort et al. (2011) also reported one important exception to the general trend: At two sites approaching the Chilean upwelling zone, forms of *E. huxleyi* with exceptionally over-calcified coccoliths dominated in naturally acidified upwelling waters, where pCO_2 reaches values more than two-fold higher than the

Deleted: $\Omega_{aragonite}$
Deleted: $\Omega_{calcite}$
Deleted: OA;
Deleted: $\Omega_{calcite}$
Deleted: $\Omega_{calcite}$
Deleted: OA
Deleted: OA
Deleted: OA responses of
Field Code Changed
Formatted: German
Deleted: OA
Deleted: s
Deleted: OA
Deleted: The ecological purpose, however, remains unclear, and it has been suggested that the coccosphere may serve for defence against grazing or parasites, for modifying light/UV levels reaching the cell, or even other purposes (Monteiro et al., 2016).
Deleted: pCO_2
Deleted: OA
Deleted: levels of calcification
Deleted: was observed in
Deleted: ,

equilibrium with present-day atmosphereic levels. Similarly, a year-long monthly survey of coccolithophore communities in the Bay of Biscay found that an over-calcified type A form dominated during the winter, when pCO_2 was highest, but contributed only a minor part to the *E. huxleyi* populations in summer, when pCO_2 was lowest (Smith et al., 2012). One explanation might be that over-calcified morphotypes are especially tolerant to such OA conditions.

The Eastern South Pacific in front of Chile and Peru presents a natural laboratory for investigating such hypotheses regarding organisms´ responses to ocean acidification. The coastal zone is naturally acidified, with surface waters frequently reaching pCO_2 levels >1000 µatm and pH values < 7.7 during upwelling events (Friederich et al., 2008; Torres et al., 2011). In this study, we surveyed the coccolithophore communities of the Chilean upwelling zone as well as adjacent coastal and offshore waters with varying pCO_2 levels and isolated *E. huxleyi* strains of dominant morphotypes. In lab-based experiments, three strains showing distinct over-calcification were compared with two moderately calcified type-A morphotypes in terms of their response to altered CO_2 and pH (400 vs. 1200 µatm pCO_2) to investigate whether CO_2 might indeed be the environmental driver selecting for the extreme overcalcified morphotypes specific to the Chilean coast.

Deleted: OA

2 Materials and Methods

2.1 Surveys

An oceanographic cruise (NBP 1305) was conducted on board R/V *Nathaniel B. Palmer* (NBP) during the early austral winter (27 June-22 July 2013) along a transitional zone from coastal to open ocean waters off central-south Peru and north Chile (Fig. 1A). A total of 24 stations were sampled between 22˚S and 13˚ S and from 70˚ W to 86˚ W (ranging from 47 to 1424 km from the coast). Central Chile coastal surveys were conducted on board the R/V Stella Maris II (Universidad Católica de Norte) during the mid-spring of 2011 (12 October) and 2012 (28 November) and aboard a rented fishing launch (18-19 November 2012) in the high pCO_2 upwelling zone in front of Tongoy Bay (TON), north Chile (~30ºS-72ºW; Fig. 1B). These two coastal surveys consisted of 7 sampling points distributed between 1 and 23 km off the coast. Another coastal sampling was conducted from a small launch (belonging to the Pontificia Universidad Católica de Chile) during the mid-spring of 2012 (10 November), in the upwelling zone in front of El Quisco Bay (QUI ~33ºS-72ºW; Fig. 1B). This coastal survey consisted of 1 sampling point located at 4 km offshore. Finally, one sampling was conducted from a rented fishing vessel during the mid-spring of 2011 (01 November), in the mesotrophic waters (MES) that surround the Juan Fernández Islands (JF; ~33ºS-78ºW; Fig. 1B).

2.2 Physical-chemical oceanographic parameters

During the NBP cruise, temperature and salinity were measured with a SBE 25 CTD (Sea-Bird Scientific, Bellevue, WA, USA) from rosette casts or from the on-board running seawater system equipped with a SBE 45 conductivity sensor and a SBE 38 temperature sensor (both from Sea-Bird Scientific). During the 2011 cruise on the R/V Stella Maris II, an SBE 19 *plus* CTD was used (data courtesy of B. Yannicelli). In other samplings, an SBE 18 plus CTD was used for water column measurements. On the 29 November 2012 cruise on the R/V Stella Maris II, surface samples were pumped continuously onboard in underway sampling and analysed with a YSI Pro30 salinometer/thermometer (YSI, Yellow Springs, OH, USA). In October 2011 and November 2012, duplicate 500 mL of surface seawater were collect into borosilicate bottles, fixed with 50µL of $HgCl_2$ saturated solution and stored until measurements of total Dissolved Inorganic Carbon (DIC) and Total Alkalinity (TA). TA was determined by potentiometric titration in an open cell (Heraldsson et al., 1997). Standardization was performed and the accuracy was controlled against a certified reference material (CRM Batch 115 bottled on September 2011) supplied by Andrew Dickson (Scripps Institution of Oceanography, http://andrew.ucsd.edu/co2qc/batches.html). The correction factor was approximately 1.002. Precision (variation between replicas) in TA always less than 0.5% (average 0.1%). DIC was determined using a fully automatic dissolved inorganic carbon analyzer (model AS-C3, Apollo SciTech, Newark, DE, USA), with variation between replicates averaging 0.1% (max. 0.3%). All the dissolved carbonate species from

Deleted: In

Deleted: stored until measurements for Total Carbon (CT)

Deleted: AT

Deleted: Total Alkalinity (

Deleted: AT)

Deleted: T

Deleted: Total carbon (CT), a.k.a. dissolved inorganic carbon (DIC),

a seawater sample were extracted as CO_2 gas by acidification and nitrogen stripping. The CO_2 gas was then quantitatively detected with an infra-red LI-7000 CO_2 Analyzer (LI-COR Environmental, Lincoln, Nebraska USA). During the expedition off Juan Fernandez (Nov 2011) pH and TA were measured in fixed samples. pH was measured on the Total Ion scale using spectrophotometric detection of m-cresol purple absorption in a 100 mm quartz cell thermally stabilized at 25.0°C (Dickson et al., 2007) with a BioSpec 1600 spectrophotometer (Shimadzu Scientific Instruments, Kyoto, Japan), with pH between replicas varying less than 0.01 units. During the NBP cruise, direct measurements of sea surface pCO_2 using NDIR detection were obtained from the ship continuous underway data acquisition system (RVDAS; courtesy of Lamont-Doherty Earth Observatory of Columbia University) in addition to TA samples.

Saturation states of aragonite (Ω_{Ar}) as well as calcite (Ω_{Ca}) and other carbonate system parameters were estimated from the DIC-TA pairs (for samplings off the central Chile coast in October 2011 and November 2012), pH-TA (for expedition off Juan Fernandez in November 2011), pCO_2-TA pairs (for NBP 1305 cruise during June-July 2013) using CO2SYS software (Pierrot et al., 2006) set with Mehrbach solubility constants (Mehrbach et al., 1973) refitted by Dickson and Millero (Dickson and Millero, 1987). Environmental parameters are provided in Table S1.

Mean sea surface temperature and chlorophyll a (Chl a) monthly climatologies (2002-2014) were obtained from the Modis Aqua satellite (Feldman, G. C., C. R. McClain, Ocean Color Web, MODIS Aqua Reprocessing R2014.0, NASA Goddard Space Flight Center. Eds. Kuring, N., Bailey, S. W. 23 Dec. 2015. http://oceancolor.gsfc.nasa.gov/) and plotted using SeaDAS (Baith et al., 2001) version 7.1 for mac OSX.

2.3 Phytoplankton analyses

Discrete seawater samples (Niskin bottles) containing planktonic assemblages were collected at various depths within the upper 150 m, depending on depth of the maximum Chl *a* fluorescence (as proxy of phytoplankton) and from the on-board seawater system when Niskin samples were not available. Duplicate 100 mL samples of seawater (previously filtered through 200 um Nitex mesh) were fixed (final concentration 1% formaldehyde, 0.05% glutaraldehyde, 10 mM borate pH 8.5) and stored at 4ºC until light microscopic examination.

Samples were sedimented in 100 mL Utermöhl chambers for 48 h prior to counting. The absolute abundance of microplankton (20-200 µm in size) and coccolithophores (ranging from 2.5-20 µm in size, but mostly comprised of species within the range 3-10 µm including *E. huxleyi*, several species of the genera *Gephyrocapsa*, and *Calcidiscus leptoporus*) were estimated with an inverted microscope (Olympus CKX41) connected to digital camera (Motic 5.0). For counts of large diatoms, thecate dinoflagellates and others planktonic cells (>50 µm in size), a 20x objective was used. For counts of small diatoms and athecate dinoflagellates (<50 µm in size) a 40x objective was used. For counts of total coccolithophores, a 40x objective was used with cross polarized light (Edmund Optics polarizers 54926 and 53347).

In parallel, duplicate 250 mL samples of seawater were filtered onto polycarbonate filters (0.2 µm pore-size; Millipore), which were dried and stored in Petri dishes until processing for identification of coccolithophore species and *E. huxleyi* morphotypes. A small cut portion of each dried filter was sputter-coated with gold. The identification and relative abundance of coccolithophore species was performed by counting a minimum of 80 coccospheres per sample by scanning electron microscopy using either a TM3000 (Hitachi High-Technologies, Tokyo, Japan) or a Quanta 250 (FEI, Hillsboro, Oregon, USA). Classification followed Young et al. (2003). To estimate the absolute abundances of each species within the Nöelaerhabdaceae family, which are difficult to distinguish by light microscopy, the relative abundance of each Nöelaerhabdaceae species determined by SEM counts was multiplied by the absolute abundance of total Nöelaerhabdaceae cells determined from light microscopy counts. SEM images were also used to measure the min. and max. coccosphere diameters and coccolith lengths of each Nöelaerhabdaceae species (ImageJ software version 1.48 for Mac OSX). Also, *E. huxleyi* cells were categorized according to Young et al. (2003), based on the distal shield and central plate of coccoliths. For analysis, they were grouped further: Lightly calcified coccoliths exhibited delicate distal shield elements that are well

Deleted: Standardization was performed with certified reference material (CRM; Bath 115 bottled on September 2011) supplied by Andrew Dickson (Scripps Institution of Oceanography).

Deleted: AT

Deleted: in

Deleted: regulated

Deleted:

Deleted: AT

Deleted: Omega

Deleted: and

Deleted: omega

Deleted: CT-AT

Deleted: AT

Deleted: AT

separated from each other extending from the central area to the outer rim, the central element was completely open, and central area elements were either lacking, lath-like, or plate-like (Fig. 2). These corresponded to the morphotypes B, B/C, C and O (Young et al., 2003; Hagino et al., 2011), a grouping that is supported by recent genetic evidence (Krueger-Hadfield et al., 2014). Moderately calcified coccoliths, corresponding to morphotype A (Young et al., 2003; Hagino et al., 2011), showed thicker distal shield elements that were fused near the central area and often at the rim but were otherwise separated, and a grill central area within a cleanly delimited tube. Two over-calcified morphotypes were observed. One corresponded to the morphotype A-overcalcified type reported in the Bay of Biscay (Smith et al., 2012) with coccolith central areas completely covered or nearly completely covered by elements of the central tube, but distal shield elements not fused (here referred to as A_CC). The second, which we refer to as R/overcalcified, corresponded to R morphotype (distal shield elements fused/slits closed), which exhibited a continuous variation from wide and open central area (Young et al., 2003) to the extreme forms, so far reported only in the Eastern South Pacific (Beaufort et al., 2011), where tube elements had completely or partially overgrown the central area.

2.4 Isolation of *E. huxleyi* strains

Clonal isolates of coccolithophores were obtained from some stations by isolation of calcified cells using an InFlux Mariner cell sorter as described previously (Von Dassow et al., 2012; Bendif et al., 2016). During the NBP cruise, the InFlux Mariner was in a portable on-board laboratory and isolation of coccolithophores occurred within six hours of sample collection. For other samplings, live seawater samples were hand-carried to Concepción in a cooler with chilled water, and calcified cells were isolated within 24h (without exposure to light or nutrient addition, to minimize possible clonal reproduction between sampling and cell isolation). Calcified strains were identified by SEM and maintained at 15˚ C (Bendif et al., 2016).

2.5 Experimental testing of *E. huxleyi* responses to high CO_2/low pH

The experiment was performed at the ocean acidification test facility of the Calfuco Marine Laboratory of the Universidad Austral de Chile (Torres et al., 2013). The aim was to investigate the effects of short term exposure to high CO_2/low pH conditions similar to those occurring in an upwelling event. The focus was on determining whether there were differences between the heavy calcified morphotypes and moderately calcified morphotypes in response to short-term exposure to CO_2, as would be expected to be experienced by phytoplankton cells from surrounding surface waters inoculating recently upwelled water, where both mooring-mounted and drifter-mounted sensors show pulses of high CO_2 over periods of about a week (Friederich et al., 2008). Experiments were conducted in temperature-controlled water baths 15˚ C, with light intensities of 75 µmol photons m^{-2} s^{-1} in a 14:10 hour light:dark cycle. Culture media were prepared from seawater collected in wintertime from the Quintay coast (central Chile), aged for >1 month, enriched with 176 µM nitrate, 7.2 µM phosphate, and with trace metals and vitamins as described for K/2 medium (Keller et al., 1987), and sterilized by filtration through 0.2 µm Stericups (Merck-Millipore, Billerica, MA, USA). Strains were acclimated to light and temperature conditions for at least two consecutive culture transfers, maintaining cell density below 200.000 cells ml^{-1} and ensuring exponential growth during the acclimation phase. Prior to inoculation, 4.5 L in 8 L cylindrical clear polycarbonate bottles (Nalgene) were continuously purged with humidified air with a pCO_2 of 400 and 1200 µatm for 24-48 hours at the experimental temperature to allow the carbonate system to equilibrate (controlled with pH readings) as described in detail in Torres et al. (2013). When pH values had stabilized, four experimental bottles per strain per treatment were inoculated at an initial density of 800 cells ml^{-1} (day 0), and aeration with the air/CO_2 mixes was continued. Daily measures of pH at 25˚ C were made potentiometrically at 25.0°C using a Metrohm 826 pH meter (nominal accuracy +/- 0.003 pH units) (Metrohm, Herisau, Switzerland) with an Aquatrode Plus with Pt1000 (Metrohm 60253100) electrode calibrated with Tris buffer using established methodology (DOE, 1994; Torres et al., 2013). Samples for TA measurement were taken on day 0 and at the end

Deleted: OA

Deleted: The OA condition (1200 µatm CO_2) was chosen to represent recently upwelled water based on Torres et al. (1999) compared to CO_2 levels in non-upwelling surface waters (400 µatm). The high CO_2 level of 1200 µatm was also chosen considering previous laboratory studies of the response of *E. huxleyi*: Results of acclimated growth rate in response to short-term changes in the carbonate system manipulated by bubbling have been reported in several studies for two R morphotype strains isolated from the Tasman Sea (where high CO_2 upwelling is not known), of which four studies reported no significant effect on growth rate of intermediate CO_2 levels (Langer et al., 2009; Shi et al., 2009; Richier et al., 2011; Rokitta and Rost, 2012) compared to one which reported a decrease at 750 µatm (Iglesias-Rodriguez et al., 2008). For other *E. huxleyi* strains, results at intermediate CO_2 levels are not consistent among studies or between strains in the same study, while all strains tested at higher levels (≤ 950 µatm) have shown slight to pronounced decreases in growth rate (Langer et al., 2009).

Deleted: at

Deleted: these

Deleted: using the indicator dye m-cresol purple with measurements of absorption at 578 nm, 434 nm, and 730 nm with a 1 cm path length as described in SOP6B (Dickson et al., 2007)

Deleted: with a BioSpec 1600 spectrophotometer (Shimadzu Scientific Instruments, Kyoto, Japan)

Deleted: Calculation of full carbonate parameters were made from pH and measures of total alkalinity (AT)

Deleted: (measured as described above) taken

of the experiment, and measured for calculation of full carbonate chemistry parameters as described above for natural seawater samples.

Daily cell counts were performed from day 2 on using a Neubauer haemocytometer (as cells were too dilute for this method on day 0). Growth rate was calculated as specific growth rates μ (day^{-1}) = $\ln(N_f/N_0)/\Delta t$, where N_0 and N_f are the initial and final cell concentrations and Δt is the time interval (days). The experimental cultures were harvested before cell concentrations reached 90,000 cells ml^{-1} to minimize changes to the carbonate system from calcification and photosynthesis based on previous studies using R morphotype strains (Rokitta and Rost, 2012). Samples for measurement of particulate organic carbon (POC) and particulate inorganic carbon (PIC) were taken by filtering four 250 ml samples on 47 mm GF/F filters (pre-combusted for overnight at 500° C) which were then dried and stored in aluminium envelopes prior to measurement of C content by the Laboratorio de Biogeoquimica y Isotopos Estables Aplicados at the Pontificia Universidad Católica using a Flash EA2000 Elemental Analyzer (Thermo Scientific, Waltham, MA, USA), with a standard error level calculated to be within 0.008 mg C according to linear regression of calibration curves using acetanilide. For each culture, total carbon (TC) was measured on two replicate filters while POC was measured on two replicate filters after treatment by exposure for 4 hours to 12N HCl fumes (Harris et al., 2001; Lorrain et al., 2003). PIC was calculated as the difference between the TC and POC. POC and PIC concentrations were normalized to cell number, and POC and PIC production rates were obtained by multiplying cell normalized POC and PIC quotas with specific growth rates. Samples were filtered and processed as described above for SEM analysis. For flow cytometry, 1.8 ml samples were fixed by adding 0.2 ml of 10% formaldehyde/0.5% glutaraldehyde, 100 mM borate pH 8.5 (which was stored frozen and thawed immediately before use).

2.5.1 SEM and flow cytometric assessments and analyses of coccoliths

Morphological analysis was performed on three replicates of each strain with a scanning electron microscope (Quanta 250) and images were analysed by ImageJ. Attached coccoliths were measured following Rosas-Navarro et al. (2016). On average, a total of 606 (min. 418) coccoliths per treatment were analysed. Coccoliths were classified into complete, incomplete and malformed (Rosas-Navarro et al., 2016). In the R/overcalcified strains, fusion of radial elements and the over-growth of inner tube elements of the distal shield complicated finer scale assessments of coccolith formation. Therefore, we were highly conservative in categorizing coccoliths, and grouped incomplete and malformed coccoliths for statistical analysis. Of all coccospheres imaged, only coccoliths were selected for measurement which were oriented upwards (towards the beam) so that coccolith length measurements were not affected by viewing angle. This meant that an average of 68 coccoliths were measured per strain per treatment. Measurements included coccolith length, the total area of the central area (defined by the inner end of distal shield radial elements), and the portion of the central area which was not covered by the inner tube.

Flow cytometry was performed using a BD InFlux equipped with a 488 nm laser and small particle detector with polarization optics. The laser, optics, and stream were aligned using 3 µm Ultra Rainbow Fluorescent Particles (Spherotech, Lake Forest, IL, USA). Trigger was set on forward scatter light with the same polarization as the laser, with trigger level adjusted for each strain to ensure that all detached coccoliths could be detected. Cells were distinguished by red fluorescence (at 692 nm; due to chlorophyll). Detached coccoliths and calcified cells were distinguished as previously described (Von Dassow et al., 2012). Briefly, calcite-containing particles are above the diagonal formed from optically inactive particles on a plot of forward scatter with polarization orthogonal to the laser versus forward scatter with polarization parallel to the laser. Also, calcite containing particles are high in side scatter. Non-calcified cells fall on the diagonal formed by other particles, including cell debris, bacteria (if present), and calibration/alignment particles. Parameters analyzed included the number of detached coccoliths, percentage of calcified cells, relative change in depolarization of forward scatter light by detached coccoliths, and relative changes in red fluorescence (due to chlorophyll) of cells. All samples for a given treatment and strain were run on the same day with the same settings.

Deleted: following protocols

Deleted: when

Deleted: were between 50,000 cells ml^{-1} and

Deleted: 100

Deleted: .

Deleted: with

Deleted: fuming

Deleted: two

Deleted: measures

Deleted: i

Deleted: litho

2.6 Statistical analysis

To test for significant correlations of environmental parameters (including carbonate chemistry) on coccolithophore community composition or *E. huxleyi* morphotype composition in the natural samples, Redundancy Analysis (RDA) was performed (see Supplement). For most analyses, we selected only data from the surface when multiple depths were available (see Supplementary Section S1 for comparison of surface to deeper samples).

Data from experimental results were analysed in Prism 6 (GraphPad Software, Inc., La Jolla, CA, USA) by 2-way ANOVA followed by Sidak post-hoc pairwise analysis with correction for multiple comparison. Prior to testing, PIC/POC ratio was $\log_2$-transformed while percentages (e.g. % area, % calcified cells) were expressed as proportions and arcsine-square-root transformed to permit use of parametric testing. Significance was judged at the $p < 0.05$ level.

3 Results

3.1 Changes in coccolithophore species and *E. huxleyi* morphotypes in natural communities versus oceanographic conditions

Surface pH (< 10 m depth) at sampling sites ranged from 7.73 (in the El Quisco 2012 sampling), to 8.11 (in the JF sampling). In terms of carbonate chemistry, the surface waters of the ESP showed a general pattern of increasing CO_2 and decreasing pH as one moves from open ocean waters to the Chilean coastal upwelling zones, however, as expected, waters were never corrosive for calcite (Fig. 3a). More generally, the NBP and JF, as well as TON and QUI surveys were conducted in a relatively low (average 411.2 ± 41.3 µatm; $N_{samples}$= 27) and high (average 696.6 ± 110 µatm; $N_{samples}$= 14) CO_2 levels, respectively.

Coccolithophore numerical abundances ranged from 1 x 10^3 cells L^{-1} to 76 x 10^3 cells L^{-1} (59 total samples) (Fig. 3b). A total of 40 coccolithophore species were found inhabiting the Eastern South Pacific during the sampling period (Table S2). Shannon diversity index ranged from 1.5 down to 0, while Fisher's alpha index ranged from 4.0 down to 0, and both indices showed coccolithophore diversity was lowest in the most acidified natural waters (Fig. 3a-b).

Five species of the Noëlaerhabdaceae family were observed, including *E. huxleyi*, *Gephyrocapsa ericsonii*, *G. muellerae*, *G. oceanica, G. parvula*, the last of which was recently re-assigned from the genus *Reticulofenestra* to the genus *Gephyrocapsa* (Bendif et al., 2016). The Noëlaerhabdaceae family numerically dominated all coccolithophore communities observed, representing between 72.2% and 100% (average 94.1% ± 6.9%) of all coccolithophores in all samples observed. The most abundant coccolithophore outside this family was *Calcidiscus leptoporus*, present at 36% of stations and ranging in relative abundance from 0.9% to 25.4% (average 5.6% ± 6.9%). Within the Noëlaerhabdaceae, *E. huxleyi* was found in every sample, and exhibited relative abundances ranging from 15.5% to 100% of total coccolithophores (Fig. 3c). While *E. huxleyi* represented up to 100% of the coccolithophore community in high-CO_2 waters on the central Chile coast (stations in groups "TON (2011)", "TON (2012)" and "QUI"), it was observed in lower relative abundances of samples taken both further off shore (NBP samples H01-U2 and JF stations) and to the north (NBP samples BB2a-BB2f), where indices of coccolithophore diversity were generally higher (Fig. 3b-c). *Gephyrocapsa ericsonii* and *G. parvula* were essentially excluded from high-CO_2 waters.

R/overcalcified morphotypes dominated *E. huxleyi* populations in high-CO_2 waters near the central Chilean coast (samples in groups "TON (2011)", "TON (2012)" and "QUI" in Fig. 3), representing on average 57.2% ± 22.9% (range 11% to 90%) (Fig. 3d). In contrast, moderately calcified A morphotype coccospheres dominated *E. huxleyi* populations in all low-CO_2 waters both further off shore (NBP samples H01-U2 and JF stations) and to waters near the coast to the north (NBP stations BB2a-BB2f). (Fig. 3d). The other overcalcified morphotype A_CC, a form characteristic of the Subtropical Front in the Western Pacific (Cubillos et al., 2007), represented less than 20% of total coccolithophores, and did not follow a clear

Formatted: Subscript

Deleted: further off shore

Deleted: strongly correlating with the

Deleted: calculated

Deleted: indices

pattern. The lightly calcified morphotypes were usually rare except in some of the samples from near Tongoy/Lengua de Vaca Point upwelling (Stations in groups "TON (2011)" and "TON (2012)" in Fig. 3d), where they seemed to be associated with intermediate CO_2 levels.

3.2 Phenotypes of *E. huxleyi* clonal isolates compared to natural populations from the high CO_2 and low CO_2 waters

Throughout the field campaigns, a total of 260 Noëlaerhabdaceae isolates were obtained and analyzed morphologically (Table 1; note that strains from stations nearby in time and space have been grouped). There was a bias towards isolating the dominant type within both the Noëlaerhabdaceae and *E. huxleyi* species complex at each station, and only 2% of the maintained isolates were from the *Gephyrocapsa* genus, suggesting that these closely related species are not as readily cultured as *E. huxleyi*. The lightly calcified morphotype also remained poorly represented in culture compared to the natural communities, and the A_CC type appeared moderately over-represented. However, among the R/overcalcified and moderately calcified A morphotypes, the dominant morphotype obtained in culture always reflected the dominant morphotype in the natural community. Three representative R/overcalcified morphotypes strains, showing different degrees of overlap of the central area, and two representative A morphotype strains from offshore waters were chosen for experimental analysis (Fig. 4).

3.3 Responses of different *E. huxleyi* morphotypes to high CO_2/low pH

Aeration with CO_2/air mixes prior to inoculation successfully equilibrated pCO_2 levels, which remained close to target levels throughout the experiment, with final pH values averaging 8.013 ± 0.029 under the control condition (400 µatm pCO_2) and 7.574 ± 0.021 high CO_2/low pH condition (1200 µatm pCO_2) (Table 2). Seawater remained supersaturated with respect to calcite ($\Omega_{calcite}$ >1) and $\Omega_{calcite}$ values achieved were in a similar range to those seen in the natural waters sampled (Fig. 2), with final values averaging across strains $\Omega_{calcite}$ = 3.252 ± 0.260 under the control condition and $\Omega_{calcite}$ = 1.423 ± 0.077 for the high CO_2/low pH condition (Table 2). Continued aeration and keeping cell concentration below 90 000 cells ml^{-1} was mostly successful in minimizing changes in carbonate system parameter. Averaging the mean values for each strain, alkalinity changed by -187 ± 132 µmol kg^{-1} (-8.24% ± 5.86%) in the control condition and -29 ± 19 µmol kg^{-1} (-1.26% ± 0.82%) under the high CO_2/low pH condition. However, for strain CHC342 the change in alkalinity under the control condition was larger (-18.64% ± 1.43%) (discussed below). This led to a lower final dissolved CO_2 (to 12.4 ± 0.2 µmol kg^{-1}) compared to the other four strains (15.0 ± 1.3 µmol kg^{-1}).

High CO_2/low pH significantly reduced the growth rate in all strains and there was no significant interaction between strain and high CO_2/low pH effects on growth rate (Fig. 5a; see Table 3 for global 2-way ANOVA statistics). High CO_2/low pH increased POC quota (POC $cell^{-1}$) in all strains. However, the interaction between strain and High CO_2/low pH was significant (Fig. 5b; Table 3). The increase in POC quota was not significant in moderately calcified strains CHC428 and CHC440, while the hyper-calcified strain CHC342 exhibited the highest POC quota and the highest increase under OA conditions. The effect of High CO_2/low pH on the POC production rate varied among strains: High CO_2/low pH increased POC production in most strains, except for the moderately calcified strain CHC428 (Fig. 5c; Table 3). However, the change in POC production was significant in post-hoc pairwise comparisons only for CHC342, in which it increased by 116% ($p < 0.0001$). Although strain CHC342, which exhibited the most overcalcified coccoliths (completely fused distal shield radial elements and central area nearly completely overgrown by tube elements), when all strains were considered neither POC quota nor POC production were consistently different in R/overcalcified vs. A morphotype strains.

PIC/POC ratios dropped under high CO_2/low pH in all strains (Fig. 5d). It is notable that the smallest changes in PIC/POC occurred in the two strains of moderately calcified morphotypes originating from offshore, low pCO_2 waters, not the strains with hyper- or heavily calcified morphotypes originating from coastal waters naturally exposed to high CO_2/low pH

Deleted: OA
Formatted: Font:Bold
Deleted: OA
Deleted: OA
Deleted: OA
Deleted: OA
Deleted: OA
Deleted: OA
Deleted: With the exception of strain CHC342, neither the
Deleted: correlated with morphotype (
Deleted:)
Deleted: OA
Deleted: OA

However, although the effect of high CO_2/low pH condition was globally significant across all strains according to a two-way ANOVA (Table 3), in pairwise post-hoc comparisons the drop in PIC/POC ratio was only significant in CHC360 ($p = 0.005$). Also, the effect of strain on PIC/POC was not significant and there was no significant interaction between strain and high CO_2/low pH (Table 3). PIC quotas varied among strains and the effect of high CO_2/low pH also differed among strains (Fig. 5e; Table 3). The highest PIC quota was recorded in the hyper calcified strain CHC342 and the lowest in the moderately calcified strain CHC440. High CO_2/low pH increased PIC quota significantly in strain CHC342 (pairwise post-hoc test, $p = 0.0039$), but did not change PIC quota or the change was not significant in other strains. PIC production varied among strains (Fig. 5f; Table 3) but there were no significant effects of high CO_2/low pH or interaction between strain and high CO_2/low pH (Table 3).

Decreases in alkalinity correlated with PIC (Table 2, Fig. S4). However, for strains CHC342 and CHC440 the drop in alkalinity was more than two fold greater than what would have been predicted from PIC under control conditions (but not under the high CO_2/low pH condition) (Supplementary Section S3, Fig. S4). When data from strains CHC342 and CHC440 were excluded, the linear relationship between measured and predicted change in alkalinity was not significantly different than 1:1 (Fig. S4).

R/overcalcified coccoliths were not more resistant to high CO_2/low pH than A morphotype coccoliths. High CO_2/low pH significantly affected at least one morphological parameter measured in all but the A morphotype strain CHC440 (Fig. 4, Fig. 6). The coccosphere diameters did not change significantly under high CO_2/low pH in any of the strains (Fig. 6d; Table 4). Coccolith lengths showed inconsistent and mostly insignificant changes among strains. In the global two-way ANOVA comparison, there was an interaction between treatment and strain (Table 4), but the only significant change under high CO_2/low pH detected by post-hoc pairwise comparisons between treatments was a small decrease in CHC428 under high CO_2/low pH (Fig. 6e; $p = 0.0334$). The percentage of the central area that was uncovered by inner tube elements increased under OA (Fig. 6f). The significant interaction between strain and treatment (Table 4) indicated that the effect of high CO_2/low pH on this parameter varied among strains. It was most pronounced in strains CHC342 and CHC352, where the inner tube elements were heavily over-grown under low pCO_2, whereas the effect was modest in the moderately calcified strains CHC428 and CHC440 (and not significant in pairwise post-hoc tests of the effect of treatment within these strains; $p > 0.05$), where the central area was mostly exposed under both conditions. The incidence of incomplete or malformed coccoliths remained very low in all strains and treatments, but high CO_2/low pH caused a modest but significant increase (Fig. 6g; Table 4), ranging from between 0 and 1.3% of coccoliths under low CO_2 to between 1.4 and 6.6% under high CO_2/low pH. This effect was greatest in R/overcalcified morphotype strains CHC342, CHC352, and CHC360, but there was no significant interaction between strain and treatment in the two-way ANOVA when all strains were considered (Table 4).

Flow cytometric analysis (see example cytogram in Fig. S5) showed significant changes in several cytometric parameters in response to high CO_2/low pH, which in some cases varied among strains (Fig. 7; Table 5). Relative chlorophyll fluorescence was increased significantly in strains CHC360, CHC440, and CHC428, but dropped significantly in CHC352 (Fig. 7a, Table 5). The proportion of cells which were calcified was high (>97%) in all strains under the 400 µatm CO_2 control treatment but dropped modestly (0.04 to 7.2%) in all strains in the OA treatment (Fig. 7b). A significant interaction was detected between strain and treatment in the proportion of cells calcified (Table 5), and this drop in response to high CO_2/low pH was greatest in strains CHC360 (average change -7.2%) and CHC440 (average change -5.4%), which were the only two strains for which the difference between treatments was judged significant in pairwise post-hoc testing. In the control CO_2 treatment, the relative abundance of detached coccoliths, relative to the number of cells, was low (11.9 $cell^{-1}$ to 14.4 $cell^{1}$) in most strains but high (63 ± 34 $cell^{-1}$) in strain CHC440. Despite significant variability among strains in the relative abundance of detached coccoliths, there were no significant changes under high CO_2/low pH (Fig. 7c; Table 5). The relative forward scatter depolarization (a proxy for the amount of calcite on a cell, see (Von Dassow et al., 2012) was decreased significantly under high CO_2/low pH (Fig. 7d; Table 5), an effect which varied among strains (Table 5) and was strongest in strain

Deleted: OA
Deleted: OA
Deleted: OA
Deleted: OA
Deleted: OA
Deleted: OA
Deleted: OA
Deleted: OA
Deleted: OA
Deleted: OA
Deleted: high CO_2
Deleted: OA condition
Deleted: OA
Deleted: OA
Deleted: OA
Deleted: OA
Deleted: s
Deleted: 7
Deleted: OA
Deleted: 8
Deleted: 8
Deleted: 8
Deleted: OA
Deleted: OA
Deleted: OA
Deleted: Fig. 8
Deleted: OA
Deleted: Fig. 8

CHC352. The relative scatter depolarization of detached coccoliths was also decreased under high CO_2/low pH (Fig. 7e; Table 5), an effect that varied among strains, and was largest in CHC352 and CHC428.

4 Discussion

While an increasing number of studies have focused on examining the potential for adaptation to ocean acidification through long-term laboratory experiments, this study has taken an alternative approach, to test for local adaptation to short-term high CO_2/low pH exposure in populations of cosmopolitan phytoplankton found in waters that experience naturally acidified conditions due to upwelling of high CO_2 water. A similar approach has recently been taken in a variety of invertebrate species (Padilla-Gamiño et al., 2016; Gaitán-Espitia et al., 2017; Vargas et al., 2017), finding both benthic/mero-planktonic animals, coralline algae, and holoplanktonic copepods do exhibit local adaptation in regions experiencing naturally high fluctuations in pH and CO_2.

This study confirms that R/overcalcified forms of *E. huxleyi* which appear exceptionally robust (as both the central area is extensively overgrown and the distal shield elements are fused) occur in the coastal zone of central to northern Chile. This was previously hinted from two sampling points/times (Beaufort et al., 2011) and now has been documented in separate years. Within the sub-tropical and tropical Eastern South Pacific, the presence of these morphotypes coincides both with high CO_2/low pH (low $\Omega_{calcite}$) as well as with lower temperature, and it is difficult to separate these two parameters. However, at the lowest end of the *E. huxleyi* temperature range, populations are often found to be dominated by more lightly calcified morphotypes (Cubillos et al., 2007), so a relationship to temperature would have to be very non-linear. More importantly, while a "type A overcalcified" type was reported in winter waters of the Bay of Biscay (Smith et al., 2012) and a "heavily calcified" type "A*" was reported in the Benguela coastal upwelling (Henderiks et al., 2012) (both exhibiting only overgrowth of the central area by tube elements but not fusion of distal shield elements), the exceptionally robust R/overcalcified forms seen near Chile have not been reported from these other upwelling systems. Therefore, we set out here to test the simplest hypothesis – focusing on a single factor – that these forms may be adapted to resist high CO_2/low pH conditions.

The use of targeted flow cytometry and cell sorting was successful in obtaining representatives of the different forms of *E. huxleyi* in mono-culture to test whether the correlation between phenotype and environment indeed reflected local adaptation. Two of the R/overcalcified strains chosen for experimental tests (CHC352 and CHC360) originated from the high CO_2 upwelling near Tongoy/Lengua de Vaca Point (Table 1). Strain CHC342 originated from Puñihuil along the outer (western) coast of Chiloe Island (41.9° S). Although we lack carbonate system data from this site, the Chiloe Island is located approximately where the West Wind Drift arrives at the continent and turns north to form the Humboldt Current System (Thiel et al., 2007), so we considered CHC342, exhibiting a highly overcalcified R morphotype, might represent the southern end of the *E. huxleyi* populations which drift north and experience high CO_2/low pH upwelling conditions. We compared these three R/overcalcified strains to two A morphotype strains isolated from low CO_2 waters at a site 1000 km from the nearest shore (NBP cruise station H10 in Fig. 1 and Fig. 3). Organisms in such waters are expected to experience very low fluctuations in pH (Hofmann et al., 2011), and so these strains were expected to exhibit low resistance to transient high CO_2/low pH conditions.

The high CO_2/low pH condition (1200 µatm CO_2) tested was chosen to represent recently upwelled water based on Torres et al. (1999) compared to CO_2 levels in non-upwelling surface waters (400 µatm). The high CO_2 level of 1200 µatm was also chosen considering previous laboratory studies of the response of *E. huxleyi*: Results of acclimated growth rate in response to short-term changes in the carbonate system manipulated by bubbling have been reported in several studies for two R morphotype strains isolated from the Tasman Sea (where high CO_2 upwelling is not known), of which four studies reported no significant effect on growth rate of intermediate CO_2 levels (Langer et al., 2009; Shi et al., 2009; Richier et al., 2011; Rokitta and Rost, 2012) compared to one which reported a decrease at 750 µatm (Iglesias-Rodriguez et al., 2008). For other

Deleted: OA
Deleted: Fig. 8
Deleted: OA
Deleted: the presence of
Deleted: exceptionally robust
Deleted: -
Deleted: ,
Deleted: and now has been documented in separate years
Deleted: Overall
Deleted: correlates
Deleted: with high CO_2 water.

E. huxleyi strains, results at intermediate CO_2 levels are not consistent among studies or between strains in the same study, while all strains tested at higher levels (≤ 950 µatm) have shown slight to pronounced decreases in growth rate (Langer et al., 2009).

The bloom-former *E. huxleyi* is often considered a fast-growing, pioneer phytoplankton species (Paasche, 2002). However, calcification is costly and most evidence suggests it may confer protective or defensive functions (Monteiro et al., 2016). Thus we considered both growth rate and calcification/morphological responses when analyzing potential adaptation. Surprisingly, we found no evidence that the exceptionally robust form was more resistant to high CO_2 than moderately calcified forms that seemed to be excluded from the high CO_2 upwelling waters.

The high CO_2/low pH treatment reduced growth rate in all strains. The decrease in growth rate was accompanied by an increase in POC quota. This might suggest that cells were getting bigger, compensating for a decreased rate of cell division (as the increase in POC production rate was not significant in 4 of the 5 strains tested). However, the decrease in growth rate was also reflected in a decrease in culture *in vivo* fluorescence (data not shown), changes in coccosphere diameter were insignificant, and changes in cellular fluorescence measured by flow cytometry were small and consistent with only a small possible increase in cell biomass (and not in all strains, as CHC352 showed a decrease in this parameter). Among the few previous studies where a period of pre-acclimation to CO_2 was not used prior to growth measurements, inconsistent and non-significant effects of growth have been seen in two R morphotype strains NZEH (PLY M219) (Shi et al., 2009) and RCC1216 (Richier et al., 2011). Another study comparing several morphotypes isolated from the Southern Ocean reported that two "A/overcalcified" strains (similar to the R morphotype strain CHC360, but with distal shield radial elements not consistently fused) were relatively resistant to high CO_2/low pH treatments compared to both A morphotype and the lighter B/C morphotype in which growth and calcification were strongly inhibited (Müller et al., 2015a). Thus the strains R/overcalcified strains tested here, originating from high CO_2 environments, were surprisingly not resistant to high CO_2. While caution is warranted in comparing the absolute resistance of the R and R/overcalcified morphotypes tested in this study to those tested in the study by Müller et al. (2015a) even when similar high CO_2/low pH treatments were tested, the robust conclusion is that the A morphotypes tested here from the Eastern South Pacific were not more sensitive than the R/overcalcified strains from neighboring high CO_2/low pH waters.

In strain CHC342, POC quota exceeded quotas previously reported in the literature for the species in response to high CO_2/low pH more than three-fold. This occurred in all four replicates, sampled at the same time as the low CO_2 replicates, so we have no evidence for this increase being a technical artefact. The increase in dissolved CO_2 in the high CO_2/low pH condition compared to the control condition was highest in strain CHC342 due to a higher consumption of alkalinity/DIC. The levels of dissolved CO_2 in the control (400 µatm pCO_2) condition for all strains fell in a range (12.4-16.6 µmol kg^{-1}) that should be saturating for photosynthesis according to one prior study (Buitenhuis et al., 1999), but sub-saturating for POC production according to a more recent study (Bach et al., 2013). The experimental variability noted might have accentuated a variability among strains in the affinity of *E. huxleyi* for photosynthetic carbon uptake. Bach et al (2013) also reported that growth rate was saturated at lower dissolved CO_2 levels than POC production. A similar increase in POC quota in response to high CO_2 has been reported in *Calcidiscus quadriperforatus* strain RCC 1168 to correlate with the production of transparent exopolysaccharides (TEP) (Diner et al., 2015), and so we suspect that the increase in POC/cell – at least in CHC342 – might correspond partly to increased TEP production under high CO_2/low pH.

As expected, PIC quotas varied among strains. CHC342, the strain showing the greatest degree of over-calcification, showed the highest PIC quota. Strain CHC440, the strain showing the coccoliths with the least percentage covering of the central area by the inner tube and the most delicate distal shield rim elements, showed the lowest PIC quota. However, the PIC quotas of CHC352, CHC360, and CHC428 were not different. The numbers of detached coccoliths per cell were similar among those three strains, but coccoliths produced by CHC428 were slightly larger, partly explaining this result. The PIC/POC ratio also did not show consistent differences among morphotypes.

Deleted: is

Deleted: serve

Deleted: ,

Deleted: OA

Deleted: similar

Deleted: OA

Deleted: used here, while growth of

Deleted: s

Deleted:

Deleted: in terms of growth rates.

Deleted: increased to over

Deleted: 3x those

Deleted: A similar increase in POC quota in response to high CO_2 has been reported in *Calcidiscus quadriperforatus* strain RCC 1168 to correlate with the production of transparent exopolysaccharides (TEP) (Diner et al., 2015), and so we suspect that the increase in POC/cell – at least in CHC342 – corresponds to increased TEP production.

Deleted:

Deleted: – considered important in determining the effect of coccolithophores on carbon export –

PIC/POC ratios decreased in all strains and all treatments, similar to what has been reported for most of the strains used in most of the previous studies (reviewed in Meyer and Riebesell 2015). However, in future studies it will be important to understand how TEP production impacts POC and PIC/POC ratios and responds to high CO_2/low pH, as has been shown in *Calcidiscus* (Diner et al., 2015). The effect of high CO_2/low pH on calcification (PIC quota and PIC production) was variable among strains, with no clear pattern related to origin or calcification, and none of these modest effects were significant except the increase in PIC quota in CHC342, the most heavily calcified strain. While calcification rate appears to be sensitive to high CO_2/low pH in most studies/strains of *E. huxleyi* (Meyer and Riebesell, 2015) despite periods of acclimation, or even adaptation over hundreds of generations (Lohbeck et al., 2012), all of the strains tested here appear to be more similar in this aspect to strains found to exhibit calcification that is relatively resistant to high CO_2/low pH (Langer et al., 2009). We did not see the dramatic loss of calcification (almost all cells were calcified in all strains and treatments) that was reported, for example, in a B/C morphotype from the Southern Ocean in response to high CO_2/low pH (Müller et al., 2015a).

We caution that the changes in alkalinity suggested that both strain CHC342 and strain CHC440 may have had approximately two-fold more PIC quota than what was directly measured under the control CO_2/pH condition. This could have occurred if the acidification of total particulate carbon samples did not effectively dissolve all calcium carbonate in these strains. This is surprising, as the geochemical analysis service that performed POC and PIC measurements followed a standard protocol recommended for both plankton samples and carbonate-rich soil samples (Harris et al., 2001; Lorrain et al., 2003) that has been previously used for measuring PIC and POC quotas in *E. huxleyi* (Zondervan et al., 2002; Sciandra et al., 2003). We speculate that perhaps the coccoliths from these strains differ from other strains in organic content in some way that makes them more resistant to acid. For example, recent comparisons have shown that the content and composition of coccolith-associated polysaccharides varies among *E. huxleyi* strains (Lee et al., 2016). However, to our knowledge, we are not aware of such an effect being reported in the literature. In any case, a possible underestimation of PIC quotas in strains CHC342 and CHC440 under the control CO_2/pH condition would mean that POC quota was overestimated under that condition, accentuating the increase in POC by high CO_2/low pH. Most importantly, it implies these strains may not have experienced an increase in PIC quota in response to high CO_2/low pH, but instead PIC quota either might have actually been maintained or decreased.

The function of coccoliths is still not certain. However, calcification is costly. It is not immediately clear if the proposed role of calcification to alleviate Ca_c^{2+} toxicity could cause the selection of overcalcified coccoliths in the high CO_2/low pH upwelling waters, as the differences in Ca_c^{2+} concentrations are vanishingly small compared to the levels at which calcification was observed to show this benefit in the lab (Müller et al., 2015b). Likewise, a possible physiological role of calcification as a carbon-concentrating mechanism to support photosynthesis in low CO_2 waters is not supported by the current balance of evidence in published literature for *E. huxleyi* (Trimborn et al., 2007) as reviewed in Monteiro et al. (2016). In any case, such an explanation could not explain why highly calcified cells would be selected for in high CO_2 waters. Most evidence suggests calcification may serve protective or defensive functions (Monteiro et al., 2016), in which case not only the rate of calcification but also the form and quality of the coccoliths would be important. Thus we also considered responses in coccolith morphology when analyzing potential adaptation.

Both microscopic and flow cytometric measures indicated that coccolith morphology was not more resistant to high CO_2/low pH conditions in the R/overcalcified strains isolated from naturally high CO_2/low pH upwellings than in the A morphotype strains isolated from far offshore waters in equilibrium with the atmosphere, that are not known to experience natural high CO_2/low pH episodes. The increase in the percentages of malformed or incomplete coccoliths in response to high CO_2/low pH was most pronounced in the R/overcalcified morphotypes, although these percentages remained low in all strains and both treatments compared to other studies. In other *E. huxleyi* morphotypes, the thickness of the tube around the coccolith central area is reported to decrease modestly under acidification conditions (Bach et al., 2012; Young et al., 2014), and a

Deleted: .
Deleted: PIC/POC ratios decreased in all strains and all treatments, similar to most studies/strains which find that this parameter is negatively affected by acidification
Deleted: acidification
Deleted:
Deleted: OA pH
Deleted: e
Deleted: acidification
Deleted: OA
Deleted: OA
Formatted: Superscript
Formatted: Subscript
Formatted: Superscript
Formatted: Subscript
Formatted: Subscript
Deleted: A consensus of b
Deleted: analysis
Deleted: natural OA conditions in
Deleted: high CO_2
Deleted: OA

similar effect was seen in the two A morphotype strains here. In our study, this effect was most pronounced, resulting in a highly eroded appearance, in the most heavily over-calcified R strains in which the tube overgrows the central area. Coccoliths are formed in intracellular compartments, and the extracellular Ω_{Ca} remained >1 in the experiments, so this must be due to effects on the formation of coccoliths, not erosion after coccolith secretion. This also shows that the degree of covering of the central area in these types depends on condition in the R morphotype, however, the principal morphotype classification of each of the 5 strains did not change, as expected if morphotype is genetically determined (Young and Westbroek, 1991). The disappearance of the underlying central area ("hollow coccoliths") reported in one study (Lefebvre et al., 2012) was not observed here. The morphological observations by SEM were supported by flow cytometric results, which also showed changes in the relative depolarization of forward scatter light both of whole coccospheres and detached coccoliths.

The observation that the morphology and quality of coccoliths of moderately calcified A morphotype strains were comparatively little affected, while R/overcalcified forms were strongly affected, does not appear consistent with the hypothesis that over-calcification of distal shield elements in the *E. huxleyi* present in naturally acidified high CO_2 water serves to compensate for high CO_2/low pH effects on coccoliths. Some other factor must select for the R/overcalcified morphotype in the coastal zone of Chile. An A morphotype ("A*") exhibiting partial and irregular extension of inner tube elements over the central area (but not closure of spaces between distal shield radial elements) was dominant in the Benguela upwelling zone (not the more extreme R/overcalcified types) (Henderiks et al., 2012), while the A_CC type, although rare in front of Chile, was dominant in the Northeast Atlantic (Bay of Biscay) in winter (Smith et al., 2012). It is interesting to speculate that high productivity conditions in eastern boundary coasts promote persistent higher abundances of grazers or phytopathogenic bacteria, against which the overcalcified coccoliths might provide better defense.

The lack of evidence for regional scale local adaptation (either in terms of growth or morphology) to short-term high CO_2/low pH conditions in *E. huxleyi* populations that are naturally exposed to pulses of naturally high CO_2/low pH upwelling conditions, contrasts with the recent findings showing adaptation to ocean acidification in estuarine habitats in invertebrates and coralline algae (Padilla-Gamiño et al., 2016; Gaitán-Espitia et al., 2017; Vargas et al., 2017), including the neritic but holoplanktonic copepod *Acartia tonsa* (Vargas et al., 2017). However, among *E. huxleyi* there is variability in response to high CO_2/low pH (Riebesell et al., 2000; Iglesias-Rodriguez et al., 2008; Langer et al., 2009; Meyer and Riebesell, 2015) that appears to correlate with morphotype and origin at least in one study (Müller et al., 2015a). This variability may already have been subject to selection. In that case, perhaps it is appropriate to consider that the present study documented a similar resistance of offshore Eastern South Pacific A morphotype strains to that of coastal strains from high CO_2/low pH waters. Although the offshore populations should be exposed less to high CO_2/low pH conditions, they might experience such conditions occasionally: Intrathermocline eddies, subsurface lenses between approximately 100 m and 500 m depth, have recently been documented to transport sub-surface waters low in dissolved O_2 in an offshore direction in the Eastern South Pacific (Andrade et al., 2014; Combes et al., 2015). These eddies would also be expected to be high CO_2/low pH, and intrusions of such water might affect organisms at the base of the euphotic zone. Such processes would still result in lower CO_2 exposure than the exposure to high CO_2/low pH occurring at the coast. Perhaps the onshore *E. huxleyi* populations, despite being exposed more frequently and more intensely to high CO_2/low pH conditions, have already reached some limit that prevents adaptation to further increases in CO_2 which limit the negative effects of these conditions on growth rate, calcification, and coccolithogenesis. Overall, the observation of consistent declines in growth rates, PIC quotas, and PIC/POC ratios, even in genotypes that naturally are exposed to high CO_2/low pH conditions, supports the prediction that PIC-associated POC export may decline under future OA conditions, potentially weakening the biological pump (Hofmann and Schellnhuber, 2009).

Deleted: a

Deleted: e

Deleted: , where

Deleted: $\Omega_{calcite}$

Deleted: , but that effect was only reported in very high cell concentrations grown with high NH_4^+

Deleted: .

Deleted: OA

Deleted:

Deleted: The function of coccoliths is still not certain,

Deleted: but they may have a role in physical defense against grazing or bacterial attack (Jaya et al., 2016; Monteiro et al., 2016).

Deleted: OA

Deleted: Eastern South Pacific *E. huxleyi* populations – despite being relatively resistant – might already be near the limit to the ability of this organism to adapt to OA

Deleted: ,

Deleted: suggesting

Deleted: this ubiquitous coccolithophore may not be able to adapt to future ocean acidification in a way that preserves ecological and biogeochemical function. The

Deleted: both

Deleted: OA

Author contributions

PD led the study, carried out sampling in field surveys, performed flow cytometric isolation of *E. huxleyi* strains, carried out statistical analysis of experimental data, supervised processing of samples by flow cytometry and electron microscopy, and wrote the manuscript. FDR conducted characterization of coccolithophore communities and *E. huxleyi* morphotype composition, analysed the relationships of coccolithophore communities and *E. huxleyi* morphotypes to environmental parameters, assisted with part of the high CO_2/low pH experiments in the Calfuco Marine Laboratory, and helped prepare the first draft of the manuscript and figures. EMB participated in field studies in 2012, helped with classification of *E. huxleyi* morphotypes, and trained and supervised FDR. in coccolithophore taxonomic classification. JDGE led experimental work in the Calfuco laboratory and provided key comments and editing of the manuscript. SR provided insights into interpretation of results and edited a draft of the manuscript. DM helped plan and perform experiments in the Calfuco lab. UJ assisted with initial plans and later interpretations. RT performed chemical analysis on seawater samples and helped set up the Calfuco Marine Laboratory experiments.

Deleted: OA

The authors declare they have no conflicts of interest.

Acknowledgements

This work was supported by the Comisión Nacional de Investigación Científica y Tecnológica of the Chilean Ministry of Education (FONDECYT grants 1110575 and 1141106, and grant CONICYT USA 20120014 to PD, a doctoral fellowship CONICYT-PCHA/Doctorado Nacional/2013- 21130158 to FDR, FONDECYT postdoc grant 312004 to DMF, and FONDEQUIP EQM130267 for the purchase of the InFlux cell sorter), by the Iniciativa Cientifica Milenio of the Chilean Ministry of Economy through the Instituto Milenio de Oceanografía de Chile (grant IC 120019), by the ASSEMBLE program (grant 227799; EMB), and by International Research Network "Diversity, Evolution and Biotechnology of Marine Algae" (GDRI N◦ 0803) of the Centre Nacional de Recherche Scientifique (PD). The authors thank J. Navarro for access to the Calfuco Marine Laboratory, V. Flores for assisting with SEM analysis, J. Beltrán for work as lab manager of the Santiago lab.

References

Andrade, I., Hormazábal, S. and Combes, V.: Intrathermocline eddies at the Juan Fernández Archipelago , southeastern Pacific Ocean, Lat. Am. J. Aquat. Res., 42(4), 888–906, doi:10.3856/vol42-issue4-fulltext-14, 2014.

Armstrong, R. A., Lee, C., Hedges, J. I., Honjo, S. and Wakeham, S. G.: A new, mechanistic model for organic carbon fluxes in the ocean based on the quantitative association of POC with ballast minerals, Deep. Res. Part II Top. Stud. Oceanogr., 49(1–3), 219–236, doi:10.1016/S0967-0645(01)00101-1, 2002.

Bach, L. T., Bauke, C., Meier, K. J. S., Riebesell, U. and Schulz, K. G.: Influence of changing carbonate chemistry on morphology and weight of coccoliths formed by Emiliania huxleyi, Biogeosciences, 9(8), 3449–3463, doi:10.5194/bg-9-3449-2012, 2012.

Bach, L. T., Mackinder, L. C. M., Schulz, K. G., Wheeler, G., Schroeder, D. C., Brownlee, C. and Riebesell, U.: Dissecting the impact of CO2 and pH on the mechanisms of photosynthesis and calcification in the coccolithophore Emiliania huxleyi, New Phytol., 199, 121–134, 2013.

Baith, K., Lindsay, R., Fu, G. and McClain, C. R.: SeaDAS, a data analysis system for ocean-color satellite sensors., Eos, Trans. Am. Geophys. Union, 82(18), 202–202, doi:10.1029/01EO00109, 2001.

Beaufort, L., Probert, I., de Garidel-Thoron, T., Bendif, E. M., Ruiz-Pino, D., Metzl, N., Goyet, C., Buchet, N., Coupel, P., Grelaud, M., Rost, B., Rickaby, R. E. M. and de Vargas, C.: Sensitivity of coccolithophores to carbonate chemistry and ocean acidification, Nature, 476(7358), 80–83, doi:10.1038/nature10295, 2011.

Bendif, E. M., Probert, I., Díaz-Rosas, F., Thomas, D., van den Engh, G., Young, J. R. and von Dassow, P.: Recent reticulate evolution in the ecologically dominant lineage of coccolithophores, Front. Microbiol., 7, 784, doi:10.3389/fmicb.2016.00784, 2016.

Brady Olson, M., Wuori, T. A., Love, B. A. and Strom, S. L.: Ocean acidification effects on haploid and diploid Emiliania huxleyi strains: Why changes in cell size matter, J. Exp. Mar. Bio. Ecol., 488, 72–82, doi:10.1016/j.jembe.2016.12.008, 2017.

Buitenhuis, E. T., Baar, H. J. W. De and Veldhuis, M. J. W.: Photosynthesis and calcification by Emiliania huxleyi (Prymnesiophyceae) as a function of inorganic carbon species, J. Phycol., 35, 949–959, 1999.

Combes, V., Hormazabal, S. and Di Lorenzo, E.: Interannual variability of the subsurface eddy field in the Southeast pacific, J. Geophys. Res. Ocean., 120, 4907–4924, doi:10.1002/2014JC010265.Received, 2015.

Cubillos, J. C., Wright, S. W., Nash, G., Salas, M. F. De, Griffiths, B., Tilbrook, B., Poisson, A. and Hallegraeff, G. M.: Calcification morphotypes of the coccolithophorid Emiliania huxleyi in the Southern Ocean: changes in 2001 to 2006 compared to historical data, Mar. Ecol. Prog. Ser., 348, 47–54, doi:10.3354/meps07058, 2007.

Von Dassow, P., Van Den Engh, G., Iglesias-Rodriguez, D. and Gittins, J. R.: Calcification state of coccolithophores can be assessed by light scatter depolarization measurements with flow cytometry, J. Plankton Res., 34(12), 1011–1027, doi:https://doi.org/10.1093/plankt/fbs061, 2012.

Dickson, A. G. and Millero, F. J.: A comparison of the equilibrium constants for the dissociation of carbonic acid in seawater media, Deep. Res. Part A. Oceanogr. Res. Pap., 34(10), 1733–1743, doi:10.1016/0198-0149(87)90021-5, 1987.

Dickson, A. G., Sabine, C. L. and Christian, J. R., Eds.: Guide to Best Practices for Ocean CO2 Measurements., PICES Special Publication 3, Victoria, BC, Canada., 2007.

Diner, R. E., Benner, I., Passow, U., Komada, T., Carpenter, E. J. and Stillman, J. H.: Negative effects of ocean acidification on calcification vary within the coccolithophore genus Calcidiscus, Mar. Biol., 162(6), 1287–1305, doi:10.1007/s00227-015-2669-x, 2015.

DOE: Handbook of methods for the analysis of the various parameters of the carbon dioxide system in sea Water., edited by A. G. Dickson and C. Goyet, ORNL/CDIAC-74., (online). [online] Available from: http://cdiac.ornl.gov/oceans/DOE_94.pdf, 1994.

Engel, A., Zondervan, I., Aerts, K., Beaufort, L., Benthien, A., Chou, L., Delille, B., Gattuso, J.-P., Harlay, J., Heemann, C., Hoffmann, L., Jacquet, S., Nejstgaard, J., Pizay, M.-D., Rochelle-newall, E., Schneider, U., Terbrueggen, A. and Riebesell, U.: Testing the direct effect of CO2 concentration on a bloom of the coccolithophorid Emiliania huxleyi in mesocosm experiments, Limnol. Oceanogr., 50(2), 493–507, 2005.

Frankignoulle, M., Canon, C. and Gattuso, J.: Marine calcification as a source of carbon dioxide: Positive feedback of increasing atmospheric CO2, Limnol. Oceanogr., 39(2), 458–462, 1994.

Friederich, G. E., Ledesma, J., Ulloa, O. and Chavez, F. P.: Air-sea carbon dioxide fluxes in the coastal southeastern tropical Pacific, Prog. Oceanogr., 79(2–4), 156–166, doi:10.1016/j.pocean.2008.10.001, 2008.

Gaitán-Espitia, J. D., Villanueva, P. A., Lopez, J., Torres, R., Navarro, J. M. and Bacigalupe, L. D.: Spatio-temporal environmental variation mediates geographical differences in phenotypic responses to ocean acidification, Biol. Lett., 13, 20160865, doi:http://dx.doi.org/10.1098/rsbl.2016.0865, 2017.

Hagino, K., Bendif, E. M., Young, J. R., Kogame, K., Probert, I., Takano, Y., Horiguchi, T., de Vargas, C. and Okada, H.: New evidence for morphological and genetic variation in the cosmopolitan coccolithophore Emiliania huxleyi (Prymnesiophyceae) from the cox1b-atp4 genes, J. Phycol., 47(5), 1164–1176, doi:10.1111/j.1529-8817.2011.01053.x, 2011.

Harris, D., Horwáth, W. R. and van Kessel, C.: Acid fumigation of soils to remove carbonates prior to total organic carbon or carbon-13 isotopic analysis, Soil Sci. Soc. Am. J., 65(6), 1853–1856, 2001.

Henderiks, J., Winter, A., Elbrächter, M., Feistel, R., Van Der Plas, A., Nausch, G. and Barlow, R.: Environmental controls on Emiliania huxleyi morphotypes in the Benguela coastal upwelling system (SE Atlantic), Mar. Ecol. Prog. Ser., 448, 51–66, doi:10.3354/meps09535, 2012.

Heraldsson, C., Anderson, L. G., Hassellöv, M., Hulth, S. and Olsson, K.: Rapid, high-precision potentiometric titration of alkalinity in ocean and sediment pore waters, Deep. Res. Part I Oceanogr. Res. Pap., 44(12), 2031–2044, doi:10.1016/S0967-0637(97)00088-5, 1997.

Hofmann, G. E., Smith, J. E., Johnson, K. S., Send, U., Levin, L. A., Micheli, F., Paytan, A., Price, N. N., Peterson, B., Takeshita, Y., Matson, P. G., de Crook, E., Kroeker, K. J., Gambi, M. C., Rivest, E. B., Frieder, C. A., Yu, P. C. and Martz, T. R.: High-frequency dynamics of ocean pH: A multi-ecosystem comparison, PLoS One, 6(12), e28983, doi:10.1371/journal.pone.0028983, 2011.

Hofmann, M. and Schellnhuber, H.-J.: Oceanic acidification affects marine carbon pump and triggers extended marine oxygen holes, Proc. Natl. Acad. Sci., 106(9), 3017–3022, doi:10.1073/pnas.0813384106, 2009.

Iglesias-Rodriguez, M. D., Halloran, P. R., Rickaby, R. E. M., Hall, I. R., Colmenero-Hidalgo, E., Gittins, J. R., Green, D. R. H., Tyrrell, T., Gibbs, S. J., von Dassow, P., Rehm, E., Armbrust, E. V. and Boessenkool, K. P.: Phytoplankton calcification in a high-CO2 world, Science (80-.)., 320(5874), 336–340, doi:10.1126/science.1154122, 2008.

Iglesias-Rodríguez, M. D., Brown, C. W., Doney, S. C., Kleypas, J., Kolber, D., Kolber, Z., Hayes, P. K. and Falkowski, P. G.: Representing key phytoplankton functional groups in ocean carbon cycle models: Coccolithophorids, Global Biogeochem. Cycles, 16(4), 47-1-47–20, doi:10.1029/2001GB001454, 2002.

Jin, P., Ding, J., Xing, T., Riebesell, U. and Gao, K.: High levels of solar radiation offset impacts of ocean acidification on calcifying and non-calcifying strains of Emiliania huxleyi, Mar. Ecol. Prog. Ser., 568, 47–58, 2017.

Keller, M. D., Selvin, R. C., Claus, W. and Guillard, R. R.: Media for the culture of oceanic ultraphytoplankton, J. Phycol., 23(4), 633–638, 1987.

Krueger-Hadfield, S. A., Balestreri, C., Schroeder, J., Highfield, A., Helaouët, P., Allum, J., Moate, R., Lohbeck, K. T., Miller, P. I., Riebesell, U., Reusch, T. B. H., Rickaby, R. E. M., Young, J. R., Hallegraeff, G., Brownlee, C. and Schroeder, D. C.: Genotyping an Emiliania huxleyi (Prymnesiophyceae) bloom event in the North Sea reveals evidence of asexual reproduction, Biogeosciences, 11, 5215–5234, doi:10.5194/bg-11-5215-2014, 2014.

Langer, G., Nehrke, G., Probert, I., Ly, J. and Ziveri, P.: Strain-specific responses of Emiliania huxleyi to changing seawater carbonate chemistry, Biogeosciences Discuss., 6(2), 4361–4383, doi:10.5194/bgd-6-4361-2009, 2009.

Lee, R. B. Y., Mavridou, D. A. I., Papadakos, G., McClelland, H. L. O. and Rickaby, R. E. M.: The uronic acid content of coccolith-associated polysaccharides provides insight into coccolithogenesis and past climate, Nat. Commun., 7, 13144, doi:10.1038/ncomms13144, 2016.

Lefebvre, S. C., Benner, I., Stillman, J. H., Parker, A. E., Drake, M. K., Rossignol, P. E., Okimura, K. M., Komada, T. and Carpenter, E. J.: Nitrogen source and pCO 2 synergistically affect carbon allocation, growth and morphology of the coccolithophore Emiliania huxleyi: Potential implications of ocean acidification for the carbon cycle, Glob. Chang. Biol., 18(2), 493–503, doi:10.1111/j.1365-2486.2011.02575.x, 2012.

Litchman, E., de Tezanos Pinto, P., Edwards, K. F., Klausmeier, C. A., Kremer, C. T. and Thomas, M. K.: Global biogeochemical impacts of phytoplankton: A trait-based perspective, J. Ecol., 103(6), 1384–1396, doi:10.1111/1365-2745.12438, 2015.

Lohbeck, K. T., Riebesell, U. and Reusch, T. B. H.: Adaptive evolution of a key phytoplankton species to ocean acidification, Nat. Geosci., 5(12), 917–917, doi:10.1038/ngeo1637, 2012.

Lorrain, A., Savoye, N., Chauvaud, L., Paulet, Y.-M. and Naulet, N.: Decarbonation and preservation method for the analysis of organic C and N contents and stable isotope ratios of low- carbonate suspended particulate material, Anal. Chim. Acta, 491, 125–133, doi:10.1016/S0003-2670(03)00815-8, 2003.

McDonald, M. J., Rice, D. P. and Desai, M. M.: Sex speeds adaptation by altering the dynamics of molecular evolution, Nature, 531(7593), 233–236, doi:10.1038/nature17143, 2016.

Mehrbach, C., Culberson, C. H., Hawley, J. E. and Pytkowicz, R. M.: Measurment of the apparent dissociation constants of carbonic acid in seawater at atmospheric pressure, Limnol. Oceanogr., 18(6), 897–907, 1973.

Meyer, J. and Riebesell, U.: Reviews and syntheses: Responses of coccolithophores to ocean acidification: A meta-analysis, Biogeosciences, 12(6), 1671–1682, doi:10.5194/bg-12-1671-2015, 2015.

Monteiro, F. M., Bach, L. T., Brownlee, C., Bown, P., Rickaby, R. E. M., Poulton, A. J., Tyrrell, T., Beaufort, L., Dutkiewicz, S., Gibbs, S., Gutowska, M. A., Lee, R., Riebesell, U., Young, J. and Ridgwell, A.: Why marine phytoplankton calcify, Sci. Adv., 2(7), e1501822–e1501822, doi:10.1126/sciadv.1501822, 2016.

Müller, M. N., Trull, T. W. and Hallegraeff, G. M.: Differing responses of three Southern Ocean Emiliania huxleyi ecotypes to changing seawater carbonate chemistry, Mar. Ecol. Prog. Ser., 531, 81–90, 2015a.

Müller, M. N., Barcelos e Ramos, J., Schulz, K. G., Riebesell, U., Kazmierczak, J., Gallo, F., MacKinder, L., Li, Y., Nesterenko, P. N., Trull, T. W. and Hallegraeff, G. M.: Phytoplankton calcification as an effective mechanism to alleviate cellular calcium poisoning, Biogeosciences, 12, 6493–6501, doi:10.5194/bg-12-6493-2015, 2015b.

Müller, M. N., Trull, T. W. and Hallegraeff, G. M.: Independence of nutrient limitation and carbon dioxide impacts on the Southern Ocean coccolithophore Emiliania huxleyi, ISME J., Advance On, 1–11, doi:10.1038/ismej.2017.53, 2017.

Orr, J. C., Fabry, V. J., Aumont, O., Bopp, L., Doney, S. C., Feely, R. A., Gnanadesikan, A., Gruber, N., Ishida, A., Joos, F., Key, R. M., Lindsay, K., Maier-Reimer, E., Matear, R., Monfray, P., Mouchet, A., Najjar, R. G., Plattner, G.-K., Rodgers, K. B., Sabine, C. L., Sarmiento, J. L., Schlitzer, R., Slater, R. D., Totterdell, I. J., Weirig, M.-F., Yamanaka, Y. and Yool, A.: Anthropogenic ocean acidification over the twenty-first century and its impact on calcifying organisms, Nature, 437(7059), 681–686, doi:10.1038/nature04095, 2005.

Paasche, E.: A review of the coccolithophorid Emiliania huxleyi (Prymnesiophyceae) with particular reference to growth, coccolith formation, and calcification-photosynthesis interactions, Phycologia, 40(6), 503–529, doi:http://dx.doi.org/10.2216/i0031-8884-40-6-503.1, 2002.

Padilla-Gamiño, J. L., Gaitán-Espitia, J. D., Kelly, M. W. and Hofmann, G. E.: Physiological plasticity and local adaptation to elevated pCO2 in calcareous algae : an ontogenetic and geographic approach, Evol. Appl., 9(2016), 1043–1053, doi:10.1111/eva.12411, 2016.

Pierrot, D., Lewis, D. E. and Wallace, D. W. R.: CO2SYS. EXE—MS excel program developed for CO2 system calculations., [online] Available from: http://cdiac.ornl.gov/ftp/co2sys, 2006.

Poulton, A. J., Young, J. R., Bates, N. R. and Balch, W. M.: Biometry of detached Emiliania huxleyi coccoliths along the Patagonian Shelf, Mar. Ecol. Prog. Ser., 443, 1–17, doi:10.3354/meps09445, 2011.

Richier, S., Fiorini, S., Kerros, M. E., von Dassow, P. and Gattuso, J. P.: Response of the calcifying coccolithophore Emiliania huxleyi to low pH/high pCO2: From physiology to molecular level, Mar. Biol., 158(3), 551–560, 2011.

Riebesell, U., Zondervan, I., Rost, B., Tortell, P. D., Zeebe, R. E. and Morel, F. M.: Reduced calcification of marine plankton in response to increased atmospheric CO2., Nature, 407(6802), 364–7, doi:10.1038/35030078, 2000.

Riebesell, U., Bach, L. T., Bellerby, R. G. J., Monsalve, J. R. B., Boxhammer, T., Czerny, J., Larsen, A., Ludwig, A. and Schulz, K. G.: Competitive fitness of a predominant pelagic calcifier impaired by ocean acidification, Nat. Geosci., 10(1), 19–23, doi:10.1038/NGEO2854, 2017.

Rokitta, S. D. and Rost, B.: Effects of CO2 and their modulation by light in the life-cycle stages of the coccolithophore Emiliania huxleyi, Limnol. Oceanogr., 57(2), 607–618, doi:10.4319/lo.2012.57.2.0607, 2012.

Rosas-Navarro, A., Langer, G. and Ziveri, P.: Temperature affects the morphology and calcification of Emiliania huxleyi strains, Biogeosciences, 13(10), 2913–2926, doi:10.5194/bg-13-2913-2016, 2016.

Sabine, C. L., Feely, R. A., Gruber, N., Key, R. M., Lee, K., Bullister, J. L., Wanninkhof, R., Wong., C. S., Wallace, D. W.

R., Tilbrook, B., Millero, F. J., Peng, T.-H., Kozyr, A., Ono, T. and Rios, A. F.: The Oceanic Sink for Anthropogenic CO2, Science (80-.)., 305(5682), 367–371, doi:10.1126/science.1097403, 2004.

Sanders, R., Morris, P. J., Poulton, A. J., Stinchcombe, M. C., Charalampopoulou, A., Lucas, M. I. and Thomalla, S. J.: Does a ballast effect occur in the surface ocean?, Geophys. Res. Lett., 37(8), 1–5, doi:10.1029/2010GL042574, 2010.

Schlüter, L., Lohbeck, K. T., Gröger, J. P., Riebesell, U. and Reusch, T. B. H.: Long-term dynamics of adaptive evolution in a globally important phytoplankton species to ocean acidification, Sci. Adv., 2(7), e1501660–e1501660, doi:10.1126/sciadv.1501660, 2016.

Sciandra, A., Harlay, J., Lefèvre, D., Lemée, R., Rimmelin, P., Denis, M. and Gattuso, J.-P.: Response of coccolithophorid Emiliania huxleyi to elevated partial pressure of CO 2 under nitrogen limitation, Mar. Ecol. Prog. Ser., 261, 111–122, 2003.

Shi, D., Xu, Y. and Morel, F. M. M.: Effects of the pH / pCO 2 control method on medium chemistry and phytoplankton growth, Biogeosciences, 6(7), 1199–1207, doi:10.5194/bg-6-1199-2009, 2009.

Smith, H. E. K., Tyrrell, T., Charalampopoulou, A., Dumousseaud, C., Legge, O. J., Birchenough, S., Pettit, L. R., Garley, R., Hartman, S. E., Hartman, M. C., Sagoo, N., Daniels, C. J., Achterberg, E. P. and Hydes, D. J.: Predominance of heavily calcified coccolithophores at low CaCO3 saturation during winter in the Bay of Biscay, Proc. Natl. Acad. Sci., 109(23), 8845–8849, doi:10.1073/pnas.1117508109, 2012.

Smith, S. V.: Parsing the oceanic calcium carbonate cycle: a net atmospheric carbon dioxide source, or a sink?, L&O e-Books. Association for the Sciences of Limnology and Oceanography Inc, Waco, TX USA., 2013.

Thiel, M., Macaya, E. C., Acuña, E., Arntz, W. E., Bastias, H., Brokordt, K., Camus, P. A., Castilla, J. C., Castro, L. R., Cortés, M., Dumont, C. P., Escribano, R., Fernández, M., Gajardo, J. A., Gaymer, C. F., Gomez, I., González, A. E., González, H. E., Haye, P. A., Illanes, J. E., Iriarte, J. L., Lancelloti, D. A., Luna-Jorquera, G., Luxoro, C., Manriquez, P. H., Marín, V., Muñoz, P., Navarretes, S. A., Perez, E., Poulin, E., Sellanes, J., Sepúlveda, H. H., Stotz, W., Tala, F., Thomas, A., Vargas, C. A., Vasquez, J. A. and VegaA, J. M. A.: The Humboldt current system of northern and central Chile Oceanographic processes, ecological interactions and socioeconomic feedback, Oceanogr. Mar. Biol., 45, 195–344, doi:10.1201/9781420050943, 2007.

Torres, R., Pantoja, S., Harada, N., González, H. E., Daneri, G., Frangopulos, M., Rutllant, J. A., Duarte, C. M., Rúiz-Halpern, S., Mayol, E. and Fukasawa, M.: Air-sea CO2 fluxes along the coast of Chile: From CO2 outgassing in central northern upwelling waters to CO2 uptake in southern Patagonian fjords, J. Geophys. Res. Ocean., 116(9), 1–17, doi:10.1029/2010JC006344, 2011.

Torres, R., Manriquez, P. H., Duarte, C., Navarro, J. M., Lagos, N. A., Vargas, C. A. and Lardies, M. A.: Evaluation of a semi-automatic system for long-term seawater carbonate chemistry manipulation, Rev. Chil. Hist. Nat., 86(4), 443–451, doi:10.4067/S0716-078X2013000400006, 2013.

Trimborn, S., Langer, G. and Rost, B.: Effect of varying calcium concentrations and light intensities on calcification and photosynthesis in Emiliania huxleyi, Limnol. Oceanogr., 52(5), 2285–2293, 2007.

Vargas, C. A., Lagos, N. A., Lardies, M. A., Duarte, C., Manríquez, P. H., Aguilera, V. M., Broitman, B., Widdicombe, S. and Dupont, S.: Species-specific responses to ocean acidification should account for local adaptation and adaptive plasticity, Nat. Ecol. Evol., 1(4), 84, doi:10.1038/s41559-017-0084, 2017.

Young, J. R. and Westbroek, P.: Genotypic variation in the coccolithophorid species Emiliania huxleyi, Mar. Micropaleontol., 18, 5–23, doi:10.1016/0377-8398(91)90004-P, 1991.

Young, J. R., Geisen, M., Cros, L., Kleijne, A., Sprengel, C., Probert, I. and Østergaard, J. B.: A guide to extant coccolithophore taxonomy, J. Nannoplankt. Res., Special Is, 1–125, 2003.

Young, J. R., Poulton, A. J. and Tyrrell, T.: Morphology of Emiliania huxleyi coccoliths on the northwestern European shelf - Is there an influence of carbonate chemistry?, Biogeosciences, 11(17), 4771–4782, doi:10.5194/bg-11-4771-2014, 2014.

Zondervan, I., Rost, B. and Riebesell, U.: Effect of CO2 concentration on the PIC/POC ratio in the coccolithophore

Emiliania huxleyi grown under light-limiting conditions and different daylengths, J. Exp. Mar. Bio. Ecol., 272, 55–70, 2002.

Formatted: Font:Italic

Table 1. Noëlaerhabdaceae strains isolated during this study. All sites near Tongoy were grouped in 2011 and in 2012, as were the sites at JF in 2011.

Site	Total strains	*E. huxleyi*				Other species		
		R/over	A_CC	A	Light	*G muel.*	*G eric.*	*G parv.*
TON 2011	132	85%	10%	2%	1%	2%	0%	0%
JF 2011	34	32%	35%	32%	0%	0%	0%	0%
TON 2012[a]	20	90%	10%	0%	0%	0%	0%	0%
Puñi. 2012[b]	10	40%	20%	40%	0%	0%	0%	0%
NBP H1	15	0%	33%	67%	0%	0%	0%	0%
NBP H10[c]	28	0%	21%	55%	24%	0%	0%	0%
NBP BB2	21	0%	33%	43%	0%	0%	5%	19%

[a] Site represented by strains CHC352 and CHC360

[b] Site represented by strain CHC342

[c] Site represented by strains CHC428 and CHC440

Table 2. Carbonate system parameters during experiment. Means ± standard deviations of experimental replicates at the time of inoculation (T_{inoc} and harvesting (T_{final}) are given. pH at the experimental temperature is calculated from measured pH at 25° C. Treatment is specified by CO_2 partial pressure (µatm) of air:CO_2 mix. pCO_2 units are µatm, alkalinity units are µmol kg^{-1}. The average ± standard deviations across strains for cell-free control bottles and mean experimental bottle values are also provided. The last two rows give the average and maximum standard deviations between replicates among all strains.

Strain	Treat.	pCO_2		Alkalinity		pH		$\Omega_{calcite}$		Dissolved $[CO_2]$	
		T_{inoc}	T_{final}	T_{inoc}	T_{final}	T_{inoc}	T_{final}	T_{inoc}	T_{final}	T_{inoc}	T_{final}
342	400	422.0±38	332±4	2260±7	1839±25	8.020±0.033	8.029±0.033	3.531±0.225	2.891±0.097	15.8±1.4	units
	1200	1314±27	1257±36	2264±5	2207±19	7.574±0.008	7.582±0.008	1.402±0.026	1.400±0.022	50.8±49.4	units
352	400	402.5±6	370.0 *	2292±13	2168 *	8.042±0.005	8.035±0.005	3.591±0.041	3.494 *	15.6±0.2	units
	1200	1226±27.6	1341±65	2274±12	2161±20	7.601±0.007	7.561±0.018	1.440±0.015	1.339±0.057	47.6±1.1	units
360	400	441.4±18.7	457.4±47.7	2270±6	2126±7	8.005±0.016	7.965±0.040	3.552±0.105	3.079±0.270	16.0±0.7	units
	1200	1186±94.7	1409±156	2289±10	2254±4	7.623±0.032	7.545±0.043	1.648±0.107	1.370±0.128	43.0±3.4	units
428	400	440.3±21.5	418.5±12.9	2261±6	2157±19	8.004±0.018	8.004±0.010	3.537±0.117	3.328±0.035	15.9±0.8	units
	1200	1259±6.4	1247±30.6	2262±4	2250±5	7.592±0.002	7.592±0.009	1.521±0.007	1.494±0.027	45.8±0.2	units
440	400	457.4±26.0	381.6±5.6	2254±6	2114±17	7.988±0.021	8.033±0.005	3.259±0.127	3.469±0.104	17.3±1.0	units
	1200	1487±32.2	1249±55.0	2261±5	2235±7	7.522±0.009	7.591±0.019	1.243±0.022	1.512±0.050	56.2±1.2	units
Ave. w/o cells	400	434.0±37.1	396.7±20.7	2265±13	2273±19	8.011±0.032	8.051±0.022	3.482±0.236	3.698±0.124	16.2±1.5	units
	1200	1286±584.2	1290±28.1	2268±8	2239±58	7.585±0.036	7.583±0.011	1.444±0.135	1.461±0.038	49.1±4.9	units
Ave. with cells	400	432.7±21.0	392.0±47.8	2267±15	2081±137	8.012±0.020	8.013±0.029	3.494±0.133	3.252±0.260	16.1±0.7	units
	1200	1294±117.1	1301±72.1	2270±12	2241±22	7.582±0.038	7.574±0.021	1.451±0.149	1.423±0.077	48.4±5.0	units
Ave. std dev.	400	22.1	17.6	8	17	0.018	0.016	0.123	0.127	0.8	units
	1200	37.5	68.6	7	11	0.012	0.020	0.035	0.057	1.4	units
Max. std dev.	400	38.2	47.7	13	25	0.033	0.040	0.225	0.270	1.4	units
	1200	94.7	156	12	20	0.033	0.043	0.107	0.128	3.4	units

*Only one alkalinity sample was analysed from the 400 pCO2 treatment for strain CHC352, as three were lost in transit between labs.

Moved (insertion) [1] ... [2]
Moved up [1]: pCO_2 units are µatm, alkalinity units are ... [3]
Deleted: ...CO_2 units are µatm, alkalinity units are µmo ... [4]
Formatted ... [5]
Deleted:
Deleted:
Formatted ... [6]
Formatted ... [9]
Formatted ... [10]
Formatted ... [7]
Formatted ... [11]
Formatted ... [8]
Formatted ... [19]
Formatted ... [20]
Formatted ... [21]
Formatted ... [22]
Formatted ... [12]
Formatted ... [18]
Formatted ... [13]
Formatted ... [14]
Formatted ... [15]
Formatted ... [16]
Formatted ... [17]
Formatted ... [30]
Formatted ... [31]
Formatted ... [32]
Formatted ... [33]
Formatted ... [23]
Formatted ... [24]
Formatted ... [25]
Formatted ... [26]
Formatted ... [27]
Formatted ... [28]
Formatted ... [29]
Formatted ... [34]
Formatted ... [35]
Formatted ... [36]
Formatted ... [37]
Formatted ... [38]
Formatted ... [39]
Deleted: 52
Formatted ... [40]
Formatted ... [41]
Formatted ... [42]
Formatted ... [43]
Formatted ... [44]
Formatted ... [45]
Formatted ... [46]
Formatted ... [47]
Formatted ... [48]

Deleted: Page Break

Table 3. Global 2-way ANOVA results for growth and biogeochemical parameters of strains exposed to high CO_2/low pH conditions versus control CO_2 treatment. PIC/POC values were log2-transformed prior to testing.

		Growth rate	POC	POC prod	PIC	PIC prod	PIC/POC
Source of variat.	Interact.	2.63 %	21.7 %	18.8 %	10.3 %	6.00 %	8.15 %
	Strain	13.7 %	62.8 %	77.5 %	71.3 %	69.2 %	10.9 %
	CO_2	60.9 %	23.0 %	9.67 %	3.68 %	2.13 %	37.8 %
F-values	Interact.	$F_{4,29} = 0.926$	$F_{4,25} = 36.1$	$F_{4,25} = 27.0$	$F_{4,25} = 3.08$	$F_{4,25} = 1.65$	$F_{4,25} = 1.15$
	Strain	$F_{4,29} = 4.83$	$F_{4,25} = 105$	$F_{4,25} = 111.0$	$F_{4,25} = 21.3$	$F_{4,25} = 19.0$	$F_{4,25} = 1.54$
	CO_2	$F_{1,29} = 85.7$	$F_{1,25} = 153$	$F_{1,25} = 55.6$	$F_{1,25} = 4.38$	$F_{1,25} = 2.33$	$F_{1,25} = 21.3$
p-values	Interact.	0.463	< 0.0001	< 0.0001	0.0343	0.194	0.358
	Strain	0.0041	< 0.0001	< 0.0001	< 0.0001	< 0.0001	0.222
	CO_2	< 0.0001	< 0.0001	< 0.0001	0.0466	0.139	0.0001

Table 4. Global 2-way ANOVA results for coccosphere and coccolith parameters of strains exposed to high CO_2/low pH conditions versus control CO_2 treatment. Proportions of central area covered and of incomplete or malformed coccoliths were arcsine-squareroot-transformed prior to testing.

		Coccosphere diameter	Coccolith length	Proportion central area covered	Proportion of coccoliths incompl. or malform.
Source of variat.	Interact.	7.58 %	34.7 %	12.3 %	4.40 %
	Strain	53.7 %	25.3 %	53.3 %	18.0 %
	CO_2	4.76 %	0.396 %	29.2 %	55.4 %
F-values	Interact.	$F_{4,19} = 1.071$	$F_{4,19} = 4.62$	$F_{4,19} = 21.9$	$F_{4,19} = 1.18$
	Strain	$F_{4,19} = 7.595$	$F_{4,19} = 3.37$	$F_{4,19} = 94.7$	$F_{4,19} = 4.83$
	CO_2	$F_{1,19} = 2.689$	$F_{1,19} = 0.211$	$F_{1,19} = 207$	$F_{1,19} = 59.6$
p-values	Interact.	0.398	0.0090	< 0.0001	0.351
	Strain	0.0008	0.0304	< 0.0001	0.0074
	CO_2	0.118	0.652	< 0.0001	< 0.0001

Table 5: Global 2-way ANOVA results for flow cytometric parameters. The percentages of calcified cells were expressed as a fraction and arcsine-squareroot-transformed prior to testing.

		Rel. red fluoresce.	% calcified	# detached coccol.	Rel. scatter depol. cells	Rel. scatter depol. detached liths
Source of variat.	Interact.	35.0 %	18.9 %	2.27 %	11.2 %	7.85 %
	Strain	34.7 %	6.42 %	67.8 %	55.8 %	57.9 %
	CO_2	13.5 %	38.7 %	1.09 %	25.4 %	22.8 %
F-values	Interact.	$F_{3,20} = 16.0$	$F_{3,20} = 3.62$	$F_{3,20} = 0.525$	$F_{3,20} = 36.5$	$F_{3,20} = 12.3$
	Strain	$F_{3,20} = 15.9$	$F_{3,20} = 1.23$	$F_{3,20} = 15.7$	$F_{3,20} = 182$	$F_{3,20} = 90.6$
	CO_2	$F_{1,20} = 18.5$	$F_{1,20} = 22.2$	$F_{1,20} = 0.757$	$F_{1,20} = 249$	$F_{1,20} = 107$
p-values	Interact.	< 0.0001	0.0309	0.670	< 0.0001	< 0.0001
	Strain	< 0.0001	0.326	< 0.0001	< 0.0001	< 0.0001
	CO_2	0.0003	0.0001	0.395	< 0.0001	< 0.0001

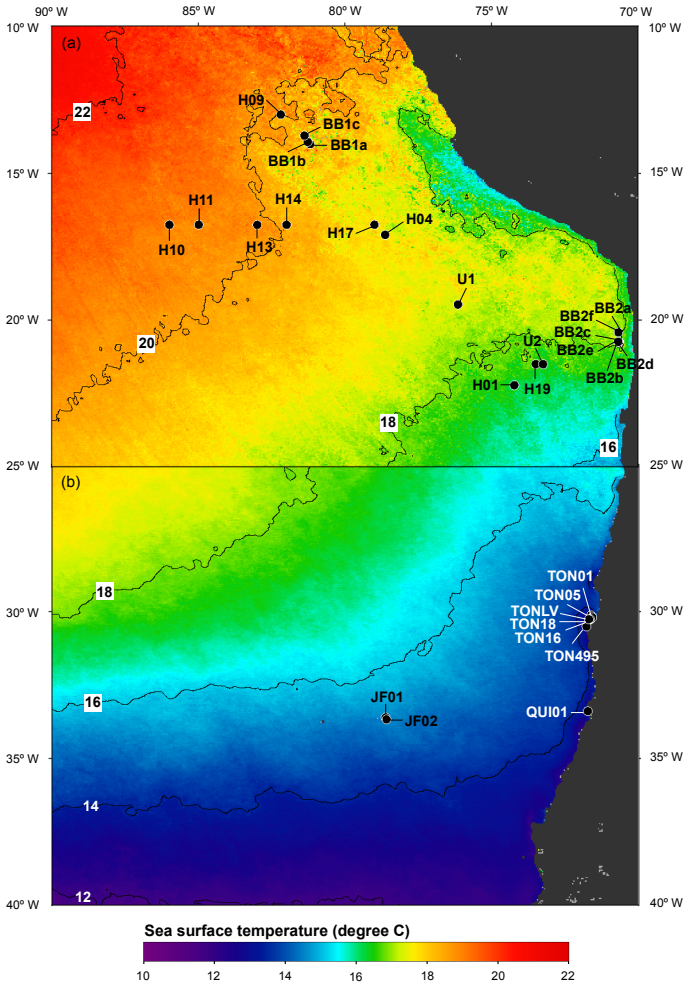

Figure 1: Map of stations sampled during NBP 1305 cruise (Jun.-Jul. 2013) (a) and in smaller field expeditions of Oct.-Nov. in 2011-2012 (b). SST climatologies (2002-2012) are plotted for the month of July (a) and October (b).

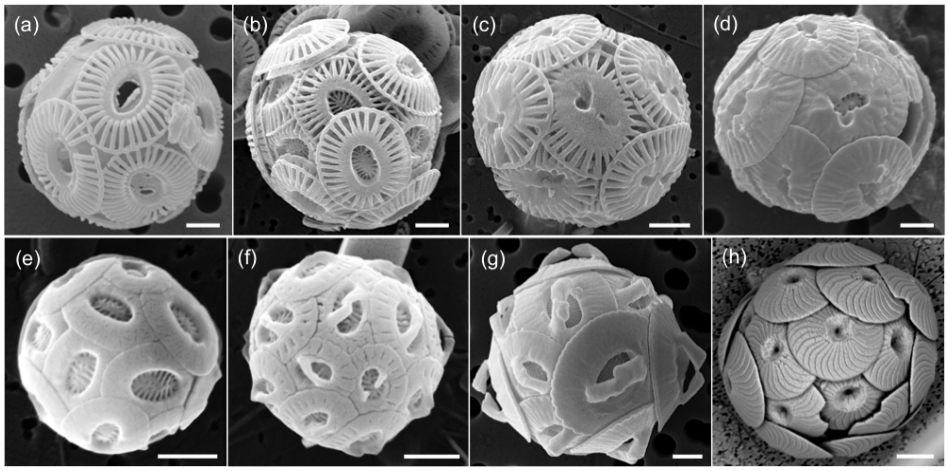

Figure 2: The most abundant coccolithophores in the SE Pacific. (a-d) Morphotypes of *E. huxleyi*: Lightly calcified (a), moderately calcified A morphotype (b), morphotype A_CC (c), morphotype R/overcalcified (d). *Gephyrocapsa parvula* (e), *G. ericsonii* (f), *G. muellerae* (g), and *Calcidiscus leptoporus*. Scale bars are 1 µm (a-g) and 3 µm in (h).

Deleted: e

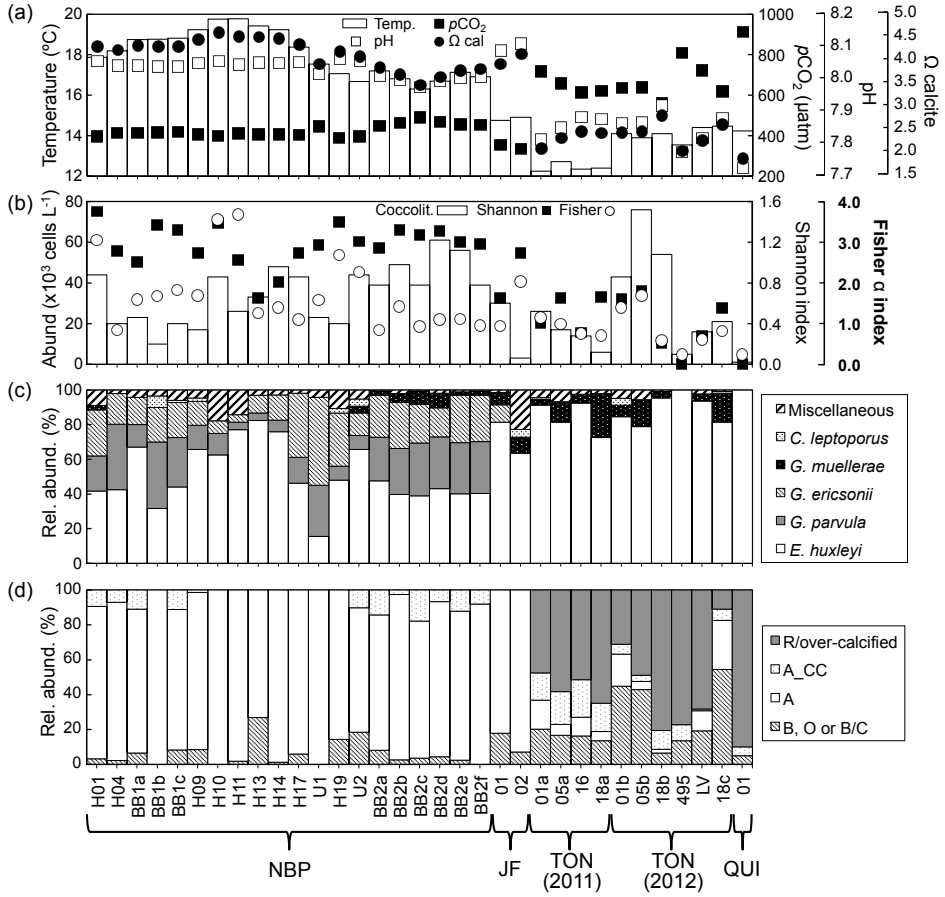

Figure 3: Environmental conditions, coccolithophore community, and *E. huxleyi* morphotypes. (a) Temperature, pH, CO_2, and $\Omega_{calcite}$. (b) Coccolithophore abundance, and Shannon and Fisher's alpha diversity indices. (c) Relative abundance of principal coccolithophore taxa. (d) Relative abundance of *E. huxleyi* morphotypes. The lightly calcified morphotypes B, O, and B/C have been grouped together.

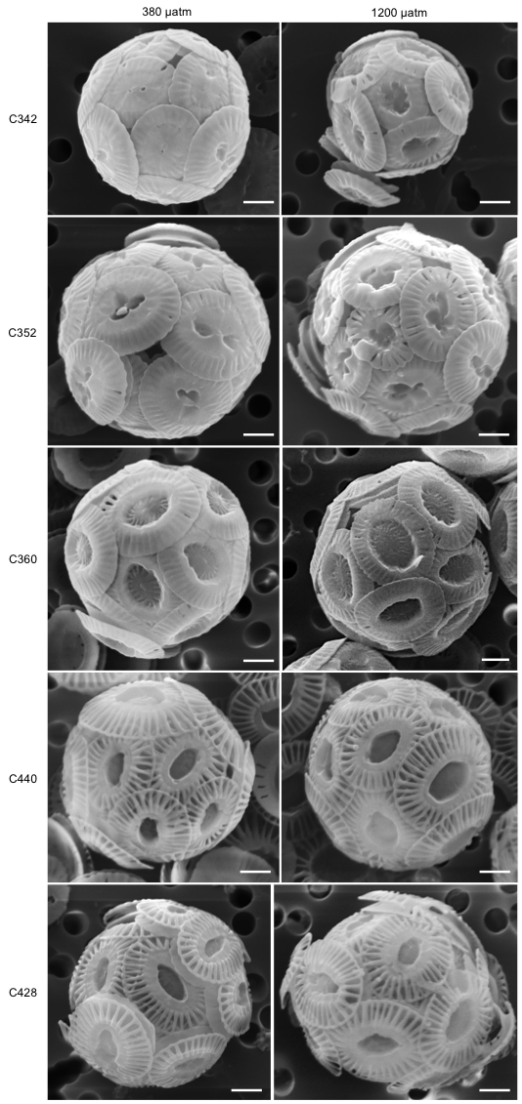

Figure 4: Representative coccospheres from each strain and treatment tested in the experiment. CHC342 was isolated from the Pacific coast of Chiloe (41.9˚ S, 74.0˚ W) in Nov. 2012, CHC352 and CHC360 were isolated from the Punta Lengua de Vaca upwelling center (30.3˚ S, 71.7˚ W) in Nov. 2012. CHC440 and CHC428 were isolated from the farthest west station in the Pacific (station H10, at 16.7˚ S, 86˚ W) during the NBP1305 cruise in Jul. 2013.

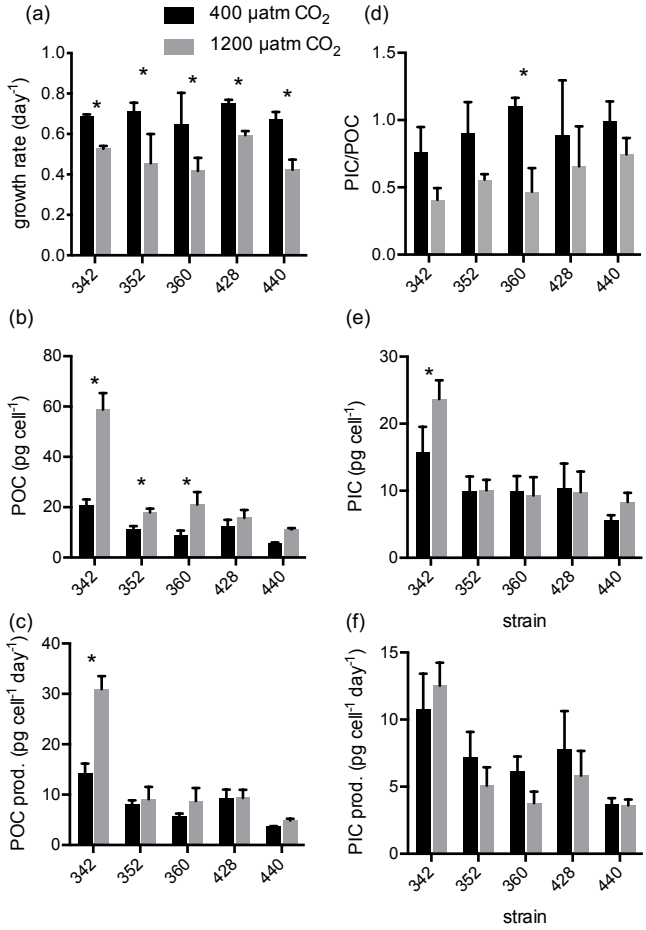

Figure 5: Growth rates (a), POC quotas (b), POC production rates (c), PIC/POC (d), PIC quotas (e), and PIC production rates (f) of *E. huxleyi* strains in response to 400 µatm (black bars) and 1200 µatm (grey bars) CO_2 treatments. See Table 3 for global two-way ANOVA results. * indicates significant difference ($p < 0.05$) in pairwise comparison between the two CO_2 treatments for a given strain, as judged by Sidak post-hoc testing with correction for multiple comparison.

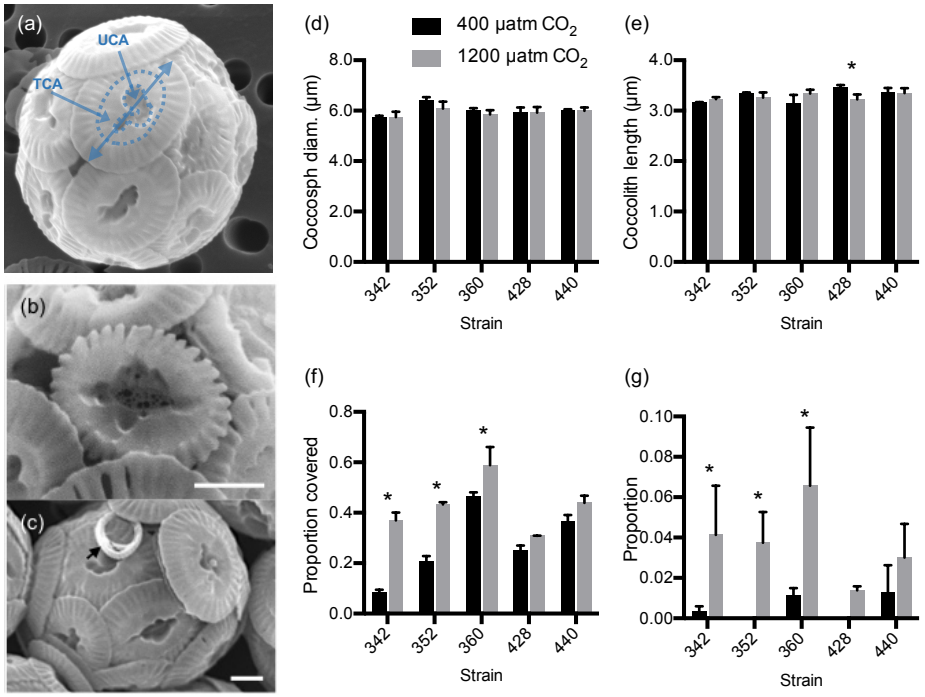

Figure 6: Effects of high CO_2/low pH conditions on coccolithophore morphology. (a) Example illustrating coccolith measurements taken including coccolith length (solid line with two arrow heads), total central area/inner tube (TCA) (defined by inner terminal of radial elements), and the part of the central area that is uncovered by tube elements (UCA). (b) Example of a coccolith classified as incomplete/malformed. (c) Example of a very incomplete coccolith (arrow). (d) Coccosphere diameters. (e) Coccolith length. (f) Proportion of central area not covered. (g) Proportion of coccoliths that were malformed or incomplete. See Table 4 for global two-way ANOVA results. * indicates significant difference ($p < 0.05$) in pairwise comparison between the two CO_2 treatments for a given strain, as judged by Sidak post-hoc testing with correction for multiple comparison.

Deleted: Page Break

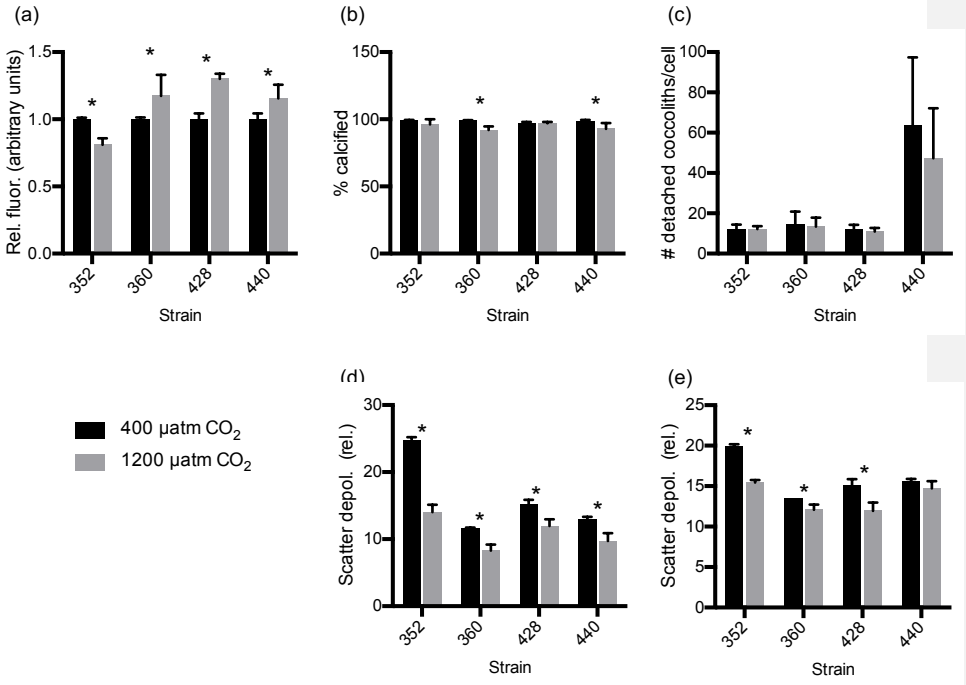

Figure 8. Effects of high CO_2 treatment on flow cytometric properties of cells and detached coccoliths for all treatments and strain. Strain CHC342 is not shown because samples were lost in transit between labs. Shown are the relative fluorescence (compared to control treatment) (a), the proportion of cells that were calcified (b), abundance of detached coccoliths divided by cell abundance (c), relative FSC (scatter depolarization) of cells (d) and detached coccoliths (e). Fluorescence and FSC units are relative and the voltage for the detector for FSC perpendicularly polarized was two-fold higher, resulting in approximately two orders of magnitude higher sensitivity. Scatter depolarization was calculated for every particle as the ratio of FSC with polarizations perpendicular vs parallel to the laser, normalized by the same ratio for non-optically active particles within the same sample. * indicates significant difference ($p < 0.05$) in pairwise comparison between the two CO_2 treatments for a given strain, as judged by Sidak post-hoc testing with correction for multiple comparison.

Page 21: [1] Formatted **Peter von Dassow** **11/29/17 10:01:00 AM**

Left: 1 cm, Right: 2.36 cm, Top: 1.65 cm, Bottom: 1.65 cm, Width: 29.7 cm, Height: 20.99 cm, Footer distance from edge: 1.57 cm

Page 21: [2] Moved from page 21 (Move #1) **Peter von Dassow** **11/29/17 1:03:00 AM**

pCO_2 units are µatm, alkalinity units are µmol kg^{-1}.

Page 21: [3] Moved to page 21 (Move #1) **Peter von Dassow** **11/29/17 1:03:00 AM**

pCO_2 units are µatm, alkalinity units are µmol kg^{-1}.

Page 21: [4] Deleted **Peter von Dassow** **11/29/17 1:12:00 AM**

Page 21: [5] Formatted **Peter von Dassow** **11/29/17 10:08:00 AM**

Font:10 pt, Not Superscript/ Subscript

Page 21: [6] Formatted **Peter von Dassow** **11/29/17 10:37:00 AM**

Indent: Left: -0.13 cm, Right: 0.02 cm

Page 21: [7] Formatted **Peter von Dassow** **11/29/17 12:36:00 AM**

Indent: Left: -0.34 cm, Right: -0.3 cm

Page 21: [8] Formatted **Peter von Dassow** **11/28/17 10:24:00 PM**

Indent: Left: -0.14 cm, Right: -0.14 cm

Page 21: [9] Formatted **Peter von Dassow** **11/29/17 12:49:00 AM**

Indent: Left: -0.19 cm, Right: -0.24 cm

Page 21: [10] Formatted **Peter von Dassow** **11/29/17 10:08:00 AM**

Font:10 pt

Page 21: [11] Formatted **Peter von Dassow** **11/29/17 10:08:00 AM**

Font:10 pt

Page 21: [12] Formatted **Peter von Dassow** **11/29/17 10:37:00 AM**

Indent: Left: -0.35 cm, Right: 0.02 cm

Page 21: [13] Formatted **Peter von Dassow** **11/29/17 10:37:00 AM**

Indent: Left: -0.34 cm, Right: -0.01 cm

Page 21: [14] Formatted **Peter von Dassow** **11/29/17 10:38:00 AM**

Centered, Indent: Left: -0.14 cm

Page 21: [15] Formatted **Peter von Dassow** **11/29/17 10:38:00 AM**

Indent: Left: -0.11 cm

Page 21: [16] Formatted **Peter von Dassow** **11/29/17 10:38:00 AM**

Indent: Left: -0.19 cm

Page 21: [17] Formatted **Peter von Dassow** **11/29/17 10:39:00 AM**

Indent: Left: -0.19 cm

Page 21: [18] Formatted **Peter von Dassow** **11/29/17 10:39:00 AM**

Indent: Left: -0.17 cm

Page 21: [19] Formatted **Peter von Dassow** **11/29/17 10:39:00 AM**

Indent: Left: -0.19 cm

Page 21: [20] Formatted **Peter von Dassow** **11/29/17 10:40:00 AM**

Right, Right: 0 cm

Page 21: [21] Formatted **Peter von Dassow** **11/29/17 10:08:00 AM**

Font:10 pt

Page 21: [22] Formatted **Peter von Dassow** **11/29/17 10:08:00 AM**

Font:10 pt

Page 21: [23] Formatted **Peter von Dassow** **11/29/17 10:37:00 AM**

Indent: Left: -0.35 cm, Right: 0.02 cm

Page 21: [24] Formatted **Peter von Dassow** **11/29/17 10:37:00 AM**

Indent: Left: -0.34 cm, Right: -0.01 cm

Page 21: [25] Formatted **Peter von Dassow** **11/29/17 10:38:00 AM**

Centered, Indent: Left: -0.14 cm

Page 21: [26] Formatted **Peter von Dassow** **11/29/17 10:38:00 AM**

Indent: Left: -0.11 cm

Page 21: [27] Formatted **Peter von Dassow** **11/29/17 10:38:00 AM**

Indent: Left: -0.19 cm

Page 21: [28] Formatted **Peter von Dassow** **11/29/17 10:39:00 AM**

Indent: Left: -0.19 cm

Page 21: [29] Formatted **Peter von Dassow** **11/29/17 10:39:00 AM**

Indent: Left: -0.17 cm

Page 21: [30] Formatted **Peter von Dassow** **11/29/17 10:39:00 AM**

Indent: Left: -0.19 cm

Page 21: [31] Formatted **Peter von Dassow** **11/29/17 10:40:00 AM**

Right, Right: 0 cm

Page 21: [32] Formatted **Peter von Dassow** **11/29/17 10:08:00 AM**

Font:10 pt

Page 21: [33] Formatted **Peter von Dassow** **11/29/17 10:08:00 AM**

Font:10 pt

Page 21: [34] Formatted **Peter von Dassow** **11/29/17 10:37:00 AM**

Indent: Left: -0.35 cm, Right: 0.02 cm

Page 21: [35] Formatted **Peter von Dassow** **11/29/17 10:37:00 AM**

Indent: Left: -0.34 cm, Right: -0.01 cm

Page 21: [36] Formatted **Peter von Dassow** **11/29/17 10:38:00 AM**

Centered, Indent: Left: -0.14 cm

Page 21: [37] Formatted **Peter von Dassow** **11/29/17 10:38:00 AM**

Indent: Left: -0.11 cm

Page 21: [38] Formatted **Peter von Dassow** **11/29/17 10:38:00 AM**

Indent: Left: -0.19 cm

Page 21: [39] Formatted **Peter von Dassow** **11/29/17 10:39:00 AM**

Indent: Left: -0.19 cm

Page 21: [40] Formatted **Peter von Dassow** **11/29/17 10:39:00 AM**

Indent: Left: -0.17 cm

Page 21: [41] Formatted **Peter von Dassow** **11/29/17 10:39:00 AM**

Indent: Left: -0.19 cm

Page 21: [42] Formatted **Peter von Dassow** **11/29/17 10:40:00 AM**

Right, Right: 0 cm

Page 21: [43] Formatted **Peter von Dassow** **11/29/17 10:08:00 AM**

Font:10 pt

Page 21: [44] Formatted **Peter von Dassow** **11/29/17 10:08:00 AM**

Font:10 pt

Page 21: [45] Formatted **Peter von Dassow** **11/29/17 10:37:00 AM**

Indent: Left: -0.35 cm, Right: 0.02 cm

Page 21: [46] Formatted **Peter von Dassow** **11/29/17 10:37:00 AM**

Indent: Left: -0.34 cm, Right: -0.01 cm

Page 21: [47] Formatted **Peter von Dassow** **11/29/17 10:38:00 AM**

Centered, Indent: Left: -0.14 cm

Page 21: [48] Formatted **Peter von Dassow** **11/29/17 10:38:00 AM**

Indent: Left: -0.11 cm

Page 21: [49] Formatted **Peter von Dassow** **11/29/17 10:38:00 AM**

Indent: Left: -0.19 cm

Page 21: [50] Formatted **Peter von Dassow** **11/29/17 10:39:00 AM**

Indent: Left: -0.19 cm

Page 21: [51] Formatted **Peter von Dassow** **11/29/17 10:39:00 AM**

Indent: Left: -0.17 cm

Page 21: [52] Formatted **Peter von Dassow** **11/29/17 10:39:00 AM**

Indent: Left: -0.19 cm

Page 21: [53] Formatted **Peter von Dassow** **11/29/17 10:40:00 AM**

Right, Right: 0 cm

Page 21: [54] Formatted **Peter von Dassow** **11/29/17 10:08:00 AM**

Font:10 pt

Page 21: [55] Formatted **Peter von Dassow** **11/29/17 10:08:00 AM**

Font:10 pt

Page 21: [56] Formatted **Peter von Dassow** **11/29/17 10:37:00 AM**

Indent: Left: -0.35 cm, Right: 0.02 cm

Page 21: [57] Formatted **Peter von Dassow** **11/29/17 10:37:00 AM**

Indent: Left: -0.34 cm, Right: -0.01 cm

Page 21: [58] Formatted **Peter von Dassow** **11/29/17 10:38:00 AM**

Centered, Indent: Left: -0.14 cm

Page 21: [59] Formatted **Peter von Dassow** **11/29/17 10:38:00 AM**

Indent: Left: -0.11 cm

Page 21: [60] Formatted **Peter von Dassow** **11/29/17 10:38:00 AM**

Indent: Left: -0.19 cm

Page 21: [61] Formatted **Peter von Dassow** **11/29/17 10:39:00 AM**

Indent: Left: -0.19 cm

Page 21: [62] Formatted **Peter von Dassow** **11/29/17 10:39:00 AM**

Indent: Left: -0.17 cm

Page 21: [63] Formatted **Peter von Dassow** **11/29/17 10:39:00 AM**

Indent: Left: -0.19 cm

Page 21: [64] Formatted **Peter von Dassow** **11/29/17 10:40:00 AM**

Right, Right: 0 cm

Page 21: [65] Formatted **Peter von Dassow** **11/29/17 10:08:00 AM**

Font:10 pt

Page 21: [66] Formatted **Peter von Dassow** **11/29/17 10:08:00 AM**

Font:10 pt

Page 21: [67] Formatted **Peter von Dassow** **11/29/17 10:37:00 AM**

Indent: Left: -0.35 cm, Right: 0.02 cm

Page 21: [68] Formatted **Peter von Dassow** **11/29/17 10:37:00 AM**

Indent: Left: -0.34 cm, Right: -0.01 cm

Page 21: [69] Formatted **Peter von Dassow** **11/29/17 10:38:00 AM**

Centered, Indent: Left: -0.14 cm

Page 21: [70] Formatted **Peter von Dassow** **11/29/17 10:38:00 AM**

Indent: Left: -0.11 cm

Page 21: [71] Formatted **Peter von Dassow** **11/29/17 10:38:00 AM**

Indent: Left: -0.19 cm

Page 21: [72] Formatted **Peter von Dassow** **11/29/17 10:39:00 AM**

Indent: Left: -0.19 cm

Page 21: [73] Formatted **Peter von Dassow** **11/29/17 10:39:00 AM**

Indent: Left: -0.17 cm

Page 21: [74] Formatted **Peter von Dassow** **11/29/17 10:39:00 AM**

Indent: Left: -0.19 cm

Page 21: [75] Formatted **Peter von Dassow** **11/29/17 10:40:00 AM**

Right, Right: 0 cm

Page 21: [76] Formatted **Peter von Dassow** **11/29/17 10:08:00 AM**

Font:10 pt

Page 21: [77] Formatted **Peter von Dassow** **11/29/17 10:08:00 AM**

Font:10 pt

Page 21: [78] Formatted **Peter von Dassow** **11/29/17 10:37:00 AM**

Indent: Left: -0.35 cm, Right: 0.02 cm

Page 21: [79] Formatted **Peter von Dassow** **11/29/17 10:37:00 AM**

Indent: Left: -0.34 cm, Right: -0.01 cm

Page 21: [80] Formatted **Peter von Dassow** **11/29/17 10:38:00 AM**

Centered, Indent: Left: -0.14 cm

Page 21: [81] Formatted **Peter von Dassow** **11/29/17 10:38:00 AM**

Indent: Left: -0.11 cm

Page 21: [82] Formatted **Peter von Dassow** **11/29/17 10:38:00 AM**

Indent: Left: -0.19 cm

Page 21: [83] Formatted **Peter von Dassow** **11/29/17 10:39:00 AM**

Indent: Left: -0.19 cm

Page 21: [84] Formatted **Peter von Dassow** **11/29/17 10:39:00 AM**

Indent: Left: -0.17 cm

Page 21: [85] Formatted **Peter von Dassow** **11/29/17 10:39:00 AM**

Indent: Left: -0.19 cm

Page 21: [86] Formatted **Peter von Dassow** **11/29/17 10:40:00 AM**

Right, Right: 0 cm

Page 21: [87] Formatted **Peter von Dassow** **11/29/17 10:08:00 AM**

Font:10 pt

Page 21: [88] Formatted **Peter von Dassow** **11/29/17 10:08:00 AM**

Font:10 pt

Page 21: [89] Formatted **Peter von Dassow** **11/29/17 10:37:00 AM**

Indent: Left: -0.35 cm, Right: 0.02 cm

Page 21: [90] Formatted **Peter von Dassow** **11/29/17 10:37:00 AM**

Indent: Left: -0.34 cm, Right: -0.01 cm

Page 21: [91] Formatted **Peter von Dassow** **11/29/17 10:38:00 AM**

Centered, Indent: Left: -0.14 cm

Page 21: [92] Formatted **Peter von Dassow** **11/29/17 10:38:00 AM**

Indent: Left: -0.11 cm

Page 21: [93] Formatted **Peter von Dassow** **11/29/17 10:38:00 AM**

Indent: Left: -0.19 cm

Page 21: [94] Formatted **Peter von Dassow** **11/29/17 10:39:00 AM**

Indent: Left: -0.19 cm

Page 21: [95] Formatted **Peter von Dassow** **11/29/17 10:39:00 AM**

Indent: Left: -0.17 cm

Page 21: [96] Formatted **Peter von Dassow** **11/29/17 10:39:00 AM**

Indent: Left: -0.19 cm

Page 21: [97] Formatted	Peter von Dassow	11/29/17 10:40:00 AM

Right, Right: 0 cm

Page 21: [98] Formatted	Peter von Dassow	11/29/17 10:08:00 AM

Font:10 pt

Page 21: [99] Formatted	Peter von Dassow	11/29/17 10:08:00 AM

Font:10 pt

Page 21: [100] Formatted	Peter von Dassow	11/29/17 10:37:00 AM

Indent: Left: -0.35 cm, Right: 0.02 cm

Page 21: [101] Formatted	Peter von Dassow	11/29/17 10:37:00 AM

Indent: Left: -0.34 cm, Right: -0.01 cm

Page 21: [102] Formatted	Peter von Dassow	11/29/17 10:38:00 AM

Centered, Indent: Left: -0.14 cm

Page 21: [103] Formatted	Peter von Dassow	11/29/17 10:38:00 AM

Indent: Left: -0.11 cm

Page 21: [104] Formatted	Peter von Dassow	11/29/17 10:38:00 AM

Indent: Left: -0.19 cm

Page 21: [105] Formatted	Peter von Dassow	11/29/17 10:39:00 AM

Indent: Left: -0.19 cm

Page 21: [106] Formatted	Peter von Dassow	11/29/17 10:39:00 AM

Indent: Left: -0.17 cm

Page 21: [107] Formatted	Peter von Dassow	11/29/17 10:39:00 AM

Indent: Left: -0.19 cm

Page 21: [108] Formatted	Peter von Dassow	11/29/17 10:40:00 AM

Right, Right: 0 cm

Page 21: [109] Formatted	Peter von Dassow	11/29/17 10:08:00 AM

Font:10 pt

Page 21: [110] Formatted	Peter von Dassow	11/29/17 10:08:00 AM

Font:10 pt

Page 21: [111] Formatted	Peter von Dassow	11/29/17 10:37:00 AM

Indent: Left: -0.35 cm, Right: 0.02 cm

Page 21: [112] Formatted	Peter von Dassow	11/29/17 10:37:00 AM

Indent: Left: -0.34 cm, Right: -0.01 cm

Page 21: [113] Formatted **Peter von Dassow** **11/29/17 10:38:00 AM**

Centered, Indent: Left: -0.14 cm

Page 21: [114] Formatted **Peter von Dassow** **11/29/17 10:38:00 AM**

Indent: Left: -0.11 cm

Page 21: [115] Formatted **Peter von Dassow** **11/29/17 10:38:00 AM**

Indent: Left: -0.19 cm

Page 21: [116] Formatted **Peter von Dassow** **11/29/17 10:39:00 AM**

Indent: Left: -0.19 cm

Page 21: [117] Formatted **Peter von Dassow** **11/29/17 10:39:00 AM**

Indent: Left: -0.17 cm

Page 21: [118] Formatted **Peter von Dassow** **11/29/17 10:39:00 AM**

Indent: Left: -0.19 cm

Page 21: [119] Formatted **Peter von Dassow** **11/29/17 10:40:00 AM**

Right, Right: 0 cm

Page 21: [120] Formatted **Peter von Dassow** **11/29/17 10:08:00 AM**

Font:10 pt

Page 21: [121] Formatted **Peter von Dassow** **11/29/17 10:08:00 AM**

Font:10 pt

Page 21: [122] Formatted **Peter von Dassow** **11/29/17 8:40:00 AM**

Font:10 pt, Font color: Black

Page 21: [123] Formatted **Peter von Dassow** **11/29/17 10:37:00 AM**

Right, Right: 0.02 cm

Page 21: [124] Formatted **Peter von Dassow** **11/29/17 10:37:00 AM**

Right, Right: -0.01 cm

Page 21: [125] Formatted **Peter von Dassow** **11/29/17 10:38:00 AM**

Right: 0 cm

Page 21: [126] Formatted **Peter von Dassow** **11/29/17 10:38:00 AM**

Right, Right: 0 cm

Page 21: [127] Formatted **Peter von Dassow** **11/29/17 10:08:00 AM**

Font:10 pt

Page 21: [128] Formatted **Peter von Dassow** **11/29/17 10:08:00 AM**

Font:10 pt

Page 21: [129] Formatted **Peter von Dassow** **11/29/17 10:37:00 AM**

Right, Right: 0.02 cm

Page 21: [130] Formatted **Peter von Dassow** **11/29/17 10:37:00 AM**

Right, Right: -0.01 cm

Page 21: [131] Formatted **Peter von Dassow** **11/29/17 10:38:00 AM**

Right: 0 cm

Page 21: [132] Formatted **Peter von Dassow** **11/29/17 10:38:00 AM**

Right, Right: 0 cm

Page 21: [133] Formatted **Peter von Dassow** **11/29/17 10:08:00 AM**

Font:10 pt

Page 21: [134] Formatted **Peter von Dassow** **11/29/17 10:08:00 AM**

Font:10 pt

Page 21: [135] Formatted **Peter von Dassow** **11/29/17 8:48:00 AM**

Font:10 pt

Page 21: [136] Formatted **Peter von Dassow** **11/29/17 10:37:00 AM**

Right, Right: 0.02 cm

Page 21: [137] Formatted **Peter von Dassow** **11/29/17 8:45:00 AM**

Font:10 pt

Page 21: [138] Formatted **Peter von Dassow** **11/29/17 10:37:00 AM**

Right, Right: -0.01 cm

Page 21: [139] Formatted **Peter von Dassow** **11/29/17 8:45:00 AM**

Font:10 pt

Page 21: [140] Formatted **Peter von Dassow** **11/29/17 10:38:00 AM**

Right: 0 cm

Page 21: [141] Formatted **Peter von Dassow** **11/29/17 8:45:00 AM**

Font:10 pt

Page 21: [142] Formatted **Peter von Dassow** **11/29/17 10:38:00 AM**

Right, Right: 0 cm

Page 21: [143] Formatted **Peter von Dassow** **11/29/17 8:45:00 AM**

Font:10 pt

Page 21: [144] Formatted **Peter von Dassow** **11/29/17 8:45:00 AM**

Font:10 pt

Page 21: [145] Formatted **Peter von Dassow** **11/29/17 8:45:00 AM**

Font:10 pt

Page 21: [146] Formatted **Peter von Dassow** **11/29/17 8:45:00 AM**

Font:10 pt

Page 21: [147] Formatted **Peter von Dassow** **11/29/17 8:45:00 AM**

Font:10 pt

Page 21: [148] Formatted **Peter von Dassow** **11/29/17 10:08:00 AM**

Font:10 pt

Page 21: [149] Formatted **Peter von Dassow** **11/29/17 10:08:00 AM**

Font:10 pt

Page 21: [150] Formatted **Peter von Dassow** **11/29/17 10:37:00 AM**

Right, Right: 0.02 cm

Page 21: [151] Formatted **Peter von Dassow** **11/29/17 8:45:00 AM**

Font:10 pt

Page 21: [152] Formatted **Peter von Dassow** **11/29/17 10:37:00 AM**

Right, Right: -0.01 cm

Page 21: [153] Formatted **Peter von Dassow** **11/29/17 8:45:00 AM**

Font:10 pt

Page 21: [154] Formatted **Peter von Dassow** **11/29/17 10:38:00 AM**

Right: 0 cm

Page 21: [155] Formatted **Peter von Dassow** **11/29/17 8:45:00 AM**

Font:10 pt

Page 21: [156] Formatted **Peter von Dassow** **11/29/17 10:38:00 AM**

Right, Right: 0 cm

Page 21: [157] Formatted **Peter von Dassow** **11/29/17 8:45:00 AM**

Font:10 pt

Page 21: [158] Formatted **Peter von Dassow** **11/29/17 8:45:00 AM**

Font:10 pt

Page 21: [159] Formatted **Peter von Dassow** **11/29/17 8:45:00 AM**

Font:10 pt

Page 21: [160] Formatted **Peter von Dassow** **11/29/17 8:45:00 AM**

Font:10 pt

Page 21: [161] Formatted **Peter von Dassow** **11/29/17 8:45:00 AM**

Font:10 pt

Page 21: [162] Formatted **Peter von Dassow** **11/29/17 10:08:00 AM**

Font:10 pt

Page 21: [163] Formatted **Peter von Dassow** **11/29/17 10:08:00 AM**

Font:10 pt

Page 21: [164] Formatted **Peter von Dassow** **11/29/17 10:03:00 AM**

Right

Page 21: [165] Formatted **Peter von Dassow** **11/29/17 10:37:00 AM**

Indent: Left: -0.35 cm, Right: 0.02 cm

Page 21: [166] Formatted **Peter von Dassow** **11/29/17 10:37:00 AM**

Indent: Left: -0.34 cm, Right: -0.01 cm

Page 21: [167] Formatted **Peter von Dassow** **11/29/17 10:38:00 AM**

Centered, Indent: Left: -0.14 cm

Page 21: [168] Formatted **Peter von Dassow** **11/29/17 10:38:00 AM**

Indent: Left: -0.11 cm

Page 21: [169] Formatted **Peter von Dassow** **11/29/17 10:38:00 AM**

Indent: Left: -0.19 cm

Page 21: [170] Formatted **Peter von Dassow** **11/29/17 10:39:00 AM**

Indent: Left: -0.19 cm

Page 21: [171] Formatted **Peter von Dassow** **11/29/17 10:39:00 AM**

Indent: Left: -0.17 cm

Page 21: [172] Formatted **Peter von Dassow** **11/29/17 10:39:00 AM**

Indent: Left: -0.19 cm

Page 21: [173] Formatted **Peter von Dassow** **11/29/17 10:40:00 AM**

Right, Right: 0 cm

Page 21: [174] Formatted **Peter von Dassow** **11/29/17 10:08:00 AM**

Font:10 pt

Page 21: [175] Formatted **Peter von Dassow** **11/29/17 10:08:00 AM**

Font:10 pt

Page 21: [176] Formatted **Peter von Dassow** **11/29/17 10:37:00 AM**

Indent: Left: -0.35 cm, Right: 0.02 cm

Page 21: [177] Formatted **Peter von Dassow** **11/29/17 10:37:00 AM**

Indent: Left: -0.34 cm, Right: -0.01 cm

Page 21: [178] Formatted **Peter von Dassow** **11/29/17 10:38:00 AM**

Centered, Indent: Left: -0.14 cm

Page 21: [179] Formatted **Peter von Dassow** **11/29/17 10:38:00 AM**

Indent: Left: -0.11 cm

Page 21: [180] Formatted **Peter von Dassow** **11/29/17 10:38:00 AM**

Indent: Left: -0.19 cm

Page 21: [181] Formatted **Peter von Dassow** **11/29/17 10:39:00 AM**

Indent: Left: -0.19 cm

Page 21: [182] Formatted **Peter von Dassow** **11/29/17 10:39:00 AM**

Indent: Left: -0.17 cm

Page 21: [183] Formatted **Peter von Dassow** **11/29/17 10:39:00 AM**

Indent: Left: -0.19 cm

Page 21: [184] Formatted **Peter von Dassow** **11/29/17 10:40:00 AM**

Right, Right: 0 cm

Page 21: [185] Formatted **Peter von Dassow** **11/29/17 10:08:00 AM**

Font:10 pt

Page 21: [186] Formatted **Peter von Dassow** **11/29/17 10:08:00 AM**

Font:10 pt

Page 21: [187] Formatted **Peter von Dassow** **11/29/17 10:03:00 AM**

Right

Page 21: [188] Formatted **Peter von Dassow** **11/29/17 10:37:00 AM**

Indent: Left: -0.35 cm, Right: 0.02 cm

Page 21: [189] Formatted **Peter von Dassow** **11/29/17 10:37:00 AM**

Indent: Left: -0.34 cm, Right: -0.01 cm

Page 21: [190] Formatted **Peter von Dassow** **11/29/17 10:38:00 AM**

Centered, Indent: Left: -0.14 cm

Page 21: [191] Formatted **Peter von Dassow** **11/29/17 10:38:00 AM**

Indent: Left: -0.11 cm

Page 21: [192] Formatted **Peter von Dassow** **11/29/17 10:38:00 AM**

Indent: Left: -0.19 cm

Page 21: [193] Formatted **Peter von Dassow** **11/29/17 10:39:00 AM**

Indent: Left: -0.19 cm

Page 21: [194] Formatted **Peter von Dassow** **11/29/17 10:39:00 AM**

Indent: Left: -0.17 cm

Page 21: [195] Formatted **Peter von Dassow** **11/29/17 10:39:00 AM**

Indent: Left: -0.19 cm

Page 21: [196] Formatted **Peter von Dassow** **11/29/17 10:40:00 AM**

Right, Right: 0 cm

Page 21: [197] Formatted **Peter von Dassow** **11/29/17 10:08:00 AM**

Font:10 pt

Page 21: [198] Formatted **Peter von Dassow** **11/29/17 10:08:00 AM**

Font:10 pt

Page 21: [199] Formatted **Peter von Dassow** **11/29/17 10:37:00 AM**

Indent: Left: -0.35 cm, Right: 0.02 cm

Page 21: [200] Formatted **Peter von Dassow** **11/29/17 10:37:00 AM**

Indent: Left: -0.34 cm, Right: -0.01 cm

Page 21: [201] Formatted **Peter von Dassow** **11/29/17 10:38:00 AM**

Centered, Indent: Left: -0.14 cm

Page 21: [202] Formatted **Peter von Dassow** **11/29/17 10:38:00 AM**

Indent: Left: -0.11 cm

Page 21: [203] Formatted **Peter von Dassow** **11/29/17 10:38:00 AM**

Indent: Left: -0.19 cm

Page 21: [204] Formatted **Peter von Dassow** **11/29/17 10:39:00 AM**

Indent: Left: -0.19 cm

Page 21: [205] Formatted **Peter von Dassow** **11/29/17 10:39:00 AM**

Indent: Left: -0.17 cm

Page 21: [206] Formatted **Peter von Dassow** **11/29/17 10:39:00 AM**

Indent: Left: -0.19 cm

Page 21: [207] Formatted **Peter von Dassow** **11/29/17 10:40:00 AM**

Right, Right: 0 cm

Page 21: [208] Formatted **Peter von Dassow** **11/29/17 10:08:00 AM**

Font:10 pt

Page 21: [209] Formatted **Peter von Dassow** **11/29/17 10:08:00 AM**

Font:10 pt